Icarus 207 (2010) 66–81

Contents lists available at ScienceDirect

Icarus

journal homepage: www.elsevier.com/locate/icarus

A meteoroid stream survey using the Canadian Meteor Orbit Radar II: Identification of minor showers using a 3D wavelet transform

P. Brown *, D.K. Wong, R.J. Weryk, P. Wiegert

Dept. of Physics and Astronomy, University of Western Ontario, London, Ontario, Canada N6A 3K7

ARTICLE INFO

Article history:
Received 23 July 2009
Revised 29 September 2009
Accepted 7 November 2009
Available online 23 November 2009

Keywords:
Meteors
Asteroids
Comets
Radar observations
Interplanetary dust

ABSTRACT

A 7 year survey using the Canadian Meteor Orbit Radar (CMOR), a specular backscattering orbital radar, has produced three million individually measured meteoroid orbits for particles with mean mass near 10^{-7} kg. We apply a 3D wavelet transform to our measured velocity vectors, partitioning them into 1° solar longitude bins while stacking all 7 years of data into a single "virtual" year to search for showers which show annual activity and last for at least 3 days. Our automated stream search algorithm has identified 117 meteor showers. We have recovered 42 of the 45 previously described streams from our first reconnaissance survey (Brown, P., Weryk, R.J., Wong, D.K., Jones, J. [2008]. Icarus 195, 317–339). Removing possible duplicate showers from the automated results leaves 109 total streams. These include 42 identified in survey I and at least 62 newly identified streams. Our large data sample and the enhanced sensitivity of the 3D wavelet search compared to our earlier survey have allowed us to extend the period of activity for several major showers. This includes detection of the Geminid shower from early November to late December and the Quadrantids from early November to mid-January. Among our newly identified streams are the Theta Serpentids which appears to be derived from 2008 KP and the Canum Venaticids which have a similar orbit to C/1975 X1 (Sato). We also find evidence that nearly 60% of all our streams are part of seven major stream complexes, linked via secular invariants.

1. Introduction

The detection of meteor showers has historically been a major enterprise in the field of meteor science. Establishing the existence and character of meteor showers provides insight into the decay processes of comets, the immediate parents to most meteor showers. Since all members of a given shower share the same parent, it becomes possible to study the parent through proxy observations of its debris. Combining observational data from meteor showers with theoretical studies of meteoroid stream evolution has led to estimates for the length of time since apparently extinct cometary bodies have last been active (e.g. 3200 Phaethon and the Geminids; Jones, 1985), dynamical explanations for large changes in activity for some showers from year-to-year (e.g. Taurids; Asher and Izumi, 1998), refined predictions related to meteor outbursts and storms (Asher, 1999) and led to lower estimates for masses of parent objects based on total mass in a meteoroid stream (Jenniskens, 2006). In some studies, detailed dynamical models are compared against shower catalogs and the resulting models verified based on whether or not a predicted shower is actually observed (cf. Babadzhanov et al., 2008). Clearly, establishing which showers exist and which are spurious becomes critical to validating such models.

While stronger showers are often measurable unambiguously with different techniques (cf. Rendtel and Arlt, 2008), the difficulty in separating coherent shower "signals" from the sporadic background has led historically to establishment of many catalogs of minor showers (see in particular the exhaustive catalog of Denning (Beech, 1990)). The lack of clear definition of what constitutes a meteor shower and combining data across multiple instrument platforms together with multiple names/designations proliferating in the literature for the same shower is a major problem.

Recently, IAU commission #22 has begun a formal procedure for recognizing and establishing meteor showers (Jenniskens et al., 2009), in response to this need and it is hoped that some regularization of accepted meteor shower lists will occur in the near future.

Here we report on an extension of our earlier radar study of meteor showers using the Canadian Meteor Orbit Radar (Brown et al., 2008, hereafter paper I). In that earlier study, we identified major showers using backscatter radar measurements of individual meteor echoes and their associated orbits. The approach taken was a conservative strategy combining single station radiant mapping techniques with 2D wavelet transforms of individually measured meteor radiants observed between 2001 and 2006. Here we ex-

* Corresponding author. Fax: +1 519 661 4085.
E-mail address: pbrown@uwo.ca (P. Brown).

0019-1035/$ - see front matter © 2009 Elsevier Inc. All rights reserved.
doi:10.1016/j.icarus.2009.11.015

pand on that earlier study, first by increasing the number of orbits examined to just over three million and extending the collection time another 2 years, to 2008. Finally, we have adopted a new search algorithm which makes use of the full meteor velocity vector with clustering examined via a 3D wavelet transform, improving our sensitivity by nearly an order of magnitude.

2. CMOR: brief review of radar hardware and analysis

The Canadian Meteor Orbit Radar (CMOR) consists of three separate interferometric radars, synchronized in transmission and receiving and operating from a single site. However, our data in this work is confined only to records made with the 29.85 MHz orbit measurement system. In paper I we summarized the main details of the system pertinent to the meteor shower survey. Technical specifications and design of the system can be found in Jones et al. (2005) and Webster et al. (2004); here we remind the reader of the most important of those details from paper I relevant to our current study.

The receive and transmit hardware for the 29.85 MHz system is based on the commercially available SKiYMET systems (Hocking et al., 2001). The basic echo detection and analysis algorithms used for the SKiYMET system are described in detail in Hocking et al. (2001). The main site has a receive antenna layout in a cross pattern with five antennas each attached to one receiver, permitting unambiguous interferometric measurement of echo directions. The main site receives signals via UHF radio links from two outlying remote stations (6.2 and 8.1 km respectively from the main site) which are fed into a sixth and seventh receiver at the main station, thus providing signals from portions of the trail not directly accessible from the specular reflection condition for the main site. For echoes detected at both outlying stations, the interferometry from the main site, when combined with the time delay from each remote site is sufficient information to permit measurement of velocity vectors for individual meteors with appropriate geometry.

The transmit and receive antenna have broad (nearly all-sky) gain patterns. The interferometric error is less than 0.5° for echoes with elevations above 30° found from comparison with optically observed meteors. More than 85% of our echo reflections have elevations above 30°, with none lower than 15°.

The effective minimal detectable signal strength at 29.85 MHz corresponds to meteors with radio magnitudes near +8 (cf. Verniani (1973) for the definition of radio meteor magnitude), while the average magnitude for echoes in our sample where orbits were measurable is +7.5. These correspond roughly to meteoroids of $\sim 10^{-7}$ kg mass for an average velocity of 30 km/s.

Our errors in velocity and radiant position vary with the echo trajectory geometry and signal-to-noise ratio of each echo. Typical values for individual radiant errors are 3° in direction and ~5% in speed. Obviously, for the stream orbits the error in the mean for these measurements is smaller than for any echo from a particular stream member. Our dominant remaining uncertainty relates to the magnitude of the deceleration correction to be applied to each measured speed. We have used the approach from Brown et al. (2004) where major showers serve as calibration points for CMOR data to compute a mean correction as a function of measured velocity and height. This average correction was applied to each echo having time-of-flight information as described in paper I. The spread in this correction means that there are often systematic errors in the expected pre-atmospheric speed; an effect manifest, for example, in several stream orbits in our survey having apparently hyperbolic orbits, a clear example of overcorrection. In all, a half-dozen cases were found in our survey where the mean orbits are computed to be hyperbolic. We find that removing the deceleration correction and using the raw average speed for the shower produces a bound orbit in each case, which we view as confirmation of a much wider spread in the true deceleration corrections than is taken into account by our simple procedure. This finding underscores the notion that no "average" meteoroid (or meteoroid stream) exists, but rather that there is a wide spread in physical characteristics among a population even one sharing a common parent (cf. Ceplecha et al., 1998).

3. Shower search methodology: application of a 3D wavelet transform to radar meteor radiant distributions

In the present study, only meteoroids whose complete velocity vector is measured are used. For these data we have the time of occurrence of the meteor plus its radiant direction and speed – sufficient information to determine its heliocentric orbit (Ceplecha, 1987). We divide our geocentric radiant measurements into 1° solar longitude bins. Each solar longitude bin has, on average, $\sim 10^4$ orbits and for each we use the geocentric radiant coordinates together with the observed geocentric speed as inputs into our wavelet transform.

From the results in paper I, we showed that for our data and the analysis approach used to measure individual orbits, the average error in measured radiant position is 3° and the spread in speeds ~5% but running as high as 10% at higher speeds. More recent simultaneous optical and radar measurements show our radiant errors to be closer to 1° on average, but these tend to be appropriate to high signal-to-noise ratio echoes and not representative of the population as a whole. Both the spread in radiant location and speed were shown in paper I to be well approximated as Gaussian distributions. We make use of these results in the form of the choice for probe sizes in our 3D wavelet transform.

The wavelet transform is often applied to datasets where clustering in several variables occurs. The power of the wavelet transform approach to identifying significance in clustering studies comes about through the ability of wavelets to be optimized based on cluster scale (Graps, 1995). In our earlier study, a 2D wavelet transform was applied to radiant location. We partitioned those individual radiant data into discrete velocity and solar longitude bins to enhance apparent clustering (presumed to be showers), but this is not optimal. In our current approach we expand the dimensionality of our search to 3D, using the spatial location of the geocentric radiant and the observed geocentric speed. By definition, shower meteors should all have radiants which cluster at or near a single value of $((\lambda - \lambda_o)_g, \beta_g, V_g)$ at a particular time. Here λ is the ecliptic longitude of the geocentric radiant, λ_o is the solar longitude at the time of occurrence of the meteor, β_g is the ecliptic latitude of the geocentric radiant and V_g is the geocentric speed. We chose to use sun-centered ecliptic longitude and ecliptic latitude as shower radiants tend to drift parallel to the ecliptic plane and show very little total drift in this coordinate system. In principle we could expand this cluster analysis to the time domain explicitly, but due to the variation in radiant collecting area with time of day, time periods less than a day produce spurious clustering. Therefore, to ensure uniformity in coverage timescales of 1 day (or integral multiples of a day) only were used for searches. For simplicity we have chosen single solar longitude degree (~1 day) time bins and keep these fixed. Experiments with longer time bins did not produce markedly improved results. We still require simple clustering in time for shower identification, however, as described later.

As in paper I, we make use of the Mexican hat mother wavelet (which is well suited to point distributions having Gaussian shapes of enhancements) to produce a wavelet transform of the form:

$$w[x_o, y_o, V_{go}] = \frac{1}{(2\pi)^{3/2}\sigma_v^{1/2} a} \int_{V_{gmin}}^{V_{gmax}} \int_{-\infty}^{+\infty} \int_{-\infty}^{+\infty} f(x, y, V_g) \times \left(3 - \frac{(x_0 - x)^2 + (y_0 - y)^2}{a^2} - \frac{(V_{go} - V_g)^2}{\sigma_v^2}\right) \times \exp\left(-0.5\left[\frac{(x_0 - x)^2 + (y_0 - y)^2}{a^2} + \frac{(V_{go} - V_g)^2}{\sigma_v^2}\right]\right) \times dx dy d v_g \quad (1)$$

where for simplicity we write $(\lambda - \lambda_o)_g = x$, $\beta_g = y$ as the spatial radiant coordinates in the plane of the sky, a is the spatial probe scale size (in degrees) of the wavelet, σ_v is the size of the velocity probe (in km/s) and $W_c(x_0, y_0, V_{g0})$ is the resulting wavelet coefficient at location (x_o, y_o, V_{go}) given a distribution of radiants, $f(x, y, V_g)$. The transform only has significant contributions from radiants that are roughly within one probe size of a particular test point; in our numerical implementation we ignore radiants more than four probe scale sizes away from the test point to reduce computation time.

To search for showers in our orbital data, we apply Eq. (1) to all our data and locate local temporal maxima in W_c. We begin by computing the median of W_c at each point (x_0,y_0,V_{g0}) taking one measure per degree of solar longitude throughout the year. The median here is found by recursively discarding points more than 3σ above the median, until a median value is found where no 3σ outliers are present. Once a median value through the entire year is computed at a particular (x_0, y_0, V_{g0}), a local maximum search is applied to each individual bin in solar longitude in turn. We define a local maxima as a point in a single solar longitude bin where the value of $W_c(x_0, y_0, V_{g0})$ is more than 3σ above the annual median. We also require that a local maximum have a minimum number of individual radiants used in the calculation of W_c (in our case this is 300). Such a requirement eliminates the problem of small number statistics which can produce many spurious maxima, particularly in the anti-apex direction. The end result of this process is a list of local maxima (together with the deviation of the maximum above the median) for a given degree of solar longitude.

Next, we attempt to link local maxima through time. Maxima are considered potentially linked if they are within 3° spatially, 10% in V_g and 2° of solar longitude. To these chains of linked maxima we then apply a further filter requiring at least three points be linked, a consistent net positive drift in right ascension and a consistent drift in declination of the radiant be present. Note this process eliminates showers of very short duration (1–2° of solar longitude), irrespective of their strength.

A final strength filter is applied whereby the median of points just before the start of the shower and just after the start of the shower is found and the largest maximum in any linked chain is required to be at least 3σ above this median limit. This final check is performed since some shower radiants have low ecliptic latitudes resulting in particular radiant directions having little or no collecting areas during certain segments of the year and in spurious (non-shower) sets of linked maxima, as the year-long median value becomes very small and not representative. Using this local background noise check, as compared to a year-long median, resulted in exclusion of 10 showers from further consideration.

Our wavelet search is first performed as described above using steps in sun-centered longitude and ecliptic latitude of 0.5° and in velocity steps of 2% for all solar longitude bins. We adopt an angular probe size of 4° and a velocity probe equivalent in size to 10% of the velocity value. Processing all three million orbits this way in the search for maxima took slightly less than 1 year of CPU time on a 2.5 GHz processor.

Once our linked maxima were identified in this initial coarse survey, we refined the linked shower maxima locations using another search limited to the region proximal to each maxima but still using the same probe sizes. In this follow-on search, the step sizes in spatial and velocity coordinates were five times smaller than the first survey allowing us to better isolate shower maxima.

Fig. 1 shows an example of a new minor shower detected with our search methodology (Chi Taurids).

4. Results

The results of our survey, containing the 117 streams identified by our analysis are given in Table 1. These streams include 42 of the 45 previously identified streams from our first survey summarized in paper I. Some of these streams may be associated with one another as a single long shower if activity temporarily drops below our threshold for a short period; our identification and linking algorithm will create two apparently distinct showers. Eliminating possible associations of this sort we have a lower limit of 109 total streams (42 identified in paper I and at least 62 newly identified streams).

This table summarizes detected showers ranked according to the solar longitude where their maximum wavelet value occurs. In addition it summarizes the duration of the shower at the 3σ level above the median background and the geocentric radiant location at the time of maximum and drift (assumed to be linear). The drift is not reported for showers of 3 days duration as drift values over such short time intervals are nearly meaningless. The wavelet coefficient at the time of maximum is given as well as the number of standard deviations the value is above the median yearly background at this point $((\lambda - \lambda_o)_g, \beta_g, V_g)$. The geocentric velocity at the time of maximum for the shower based on the wavelet peak is also provided.

Table 2 summarizes the mean orbit of the shower using the time of maximum, the geocentric radiant at the time of maximum and V_{gmax}.

In examining our total shower results (117 showers total including possible duplicates), we have been able to link 55 showers with previously adopted provisional showers of the IAU shower list (Jenniskens et al., 2009) including 42 showers from our first survey and 13 additional showers. The remaining 62 showers are not listed in the IAU shower catalog, though some have been tentatively identified in other surveys (e.g. Molau, 2007), but not formally recognized. Note that in many cases for the showers subjectively linked from our work to the IAU list, substantial differences in radiant, time of maximum and/or velocity were encountered.

Fig. 2 shows the distribution of showers throughout the year as a function of their velocity and strength. The major showers are readily visible in this plot. Also notable are the numerous weak showers which persist for long periods. The paucity of lower velocity showers (below 20 km/s) is unlikely a real feature, but rather an artifact of the strong velocity bias of our radar data, with the production of scattering electrons from meteoroid ablation varying strongly as a function of v and dropping very rapidly at velocities <20 km/s (cf. Jones, 1997) coupled with the generally larger radiant areas expected for low velocity streams (Kresak and Porubcan, 1970). One consequence of this selection effect is that we are unlikely to detect many asteroidal meteoroid streams using our current search criteria.

Finally, the radiant locations in sun-centered coordinates at the time of each shower's maximum are shown in Fig. 3. Here the shower locations are plotted relative to the main sporadic radiant sources (cf. Jones and Brown, 1993). While many showers do occur in one of the main sporadic sources, interestingly, a large number of our identified showers occur along two "arcs" connecting the north toroidal source with the helion and anti-helion sporadic sources. We believe this radiant distribution to be indicative of a

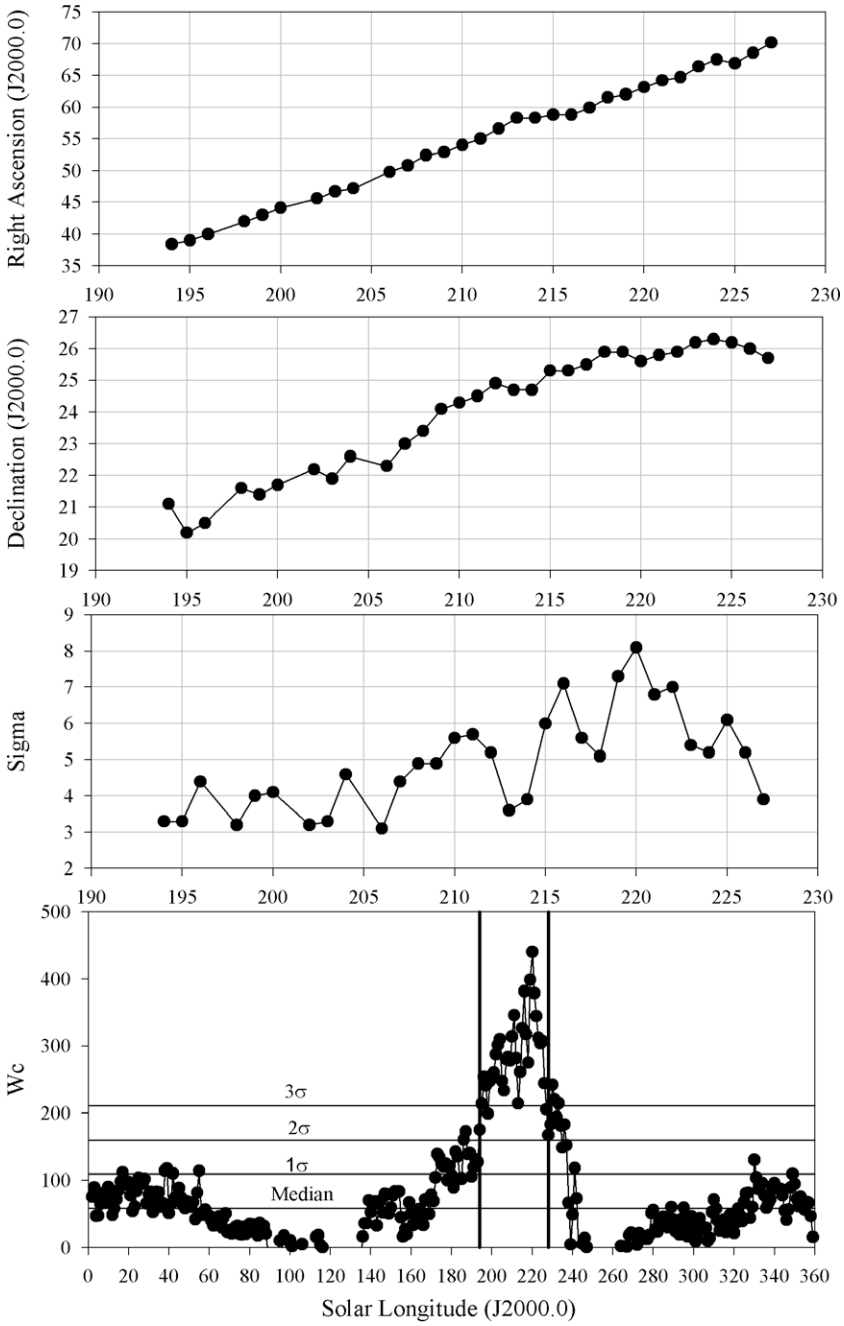

Fig. 1. Example of a new minor shower (Chi Taurids) identified with our linking procedure. The top plot shows the drift in right ascension, the next plot the drift in declination and the third plot shows the excursion in the value of the wavelet coefficient in units of standard deviations for the shower at each solar longitude interval above the yearly median value at that radiant location. The bottom-most plot shows the wavelet coefficient computed throughout the year at the sun-centered radiant location at the time of maximum of the shower ($\lambda = 220°$); note the change in the x-axis scale between the bottom-most plot and the other three plots. The interval in which our algorithm identified the shower is shown by vertical bold lines. The median background and standard deviations above this median level are also given. There clearly is some activity persisting beyond these limits; however as the excursions in strength are below 3σ relative to the fluctuations averaged over the entire year outside our window, we do not track the shower outside this interval. Note that this shower may be associated with the σ-Arietids (Jenniskens, 2006).

related complex of showers potentially with a common progenitor – we will comment in the next section in detail on the significance of this result.

5. Discussion

The results of our survey suggest that some of the streams detected are part of a broader complex of showers. It has been assumed that the sporadic sources are the result of ever broadening and merging of older streams (cf. Jones and Brown, 1993). That some streams are relatively old (e.g. Perseids) has been established through simulations (Brown and Jones, 1998), while other streams are unquestionably very young based solely on their present activity variations and short periods of activity, e.g. the October Draconids (cf. Jenniskens, 2006). Younger streams often may be linked to parent objects purely on the basis of orbital similarity. Such cases are possible because these stream meteoroids have evolved through less than ~1 precession cycle and remain on orbits similar to those at their ejection epoch. In contrast, much older streams become widely spread out in both nodal longitude

Table 1
Summary table of showers found using our search methodology, arranged according to the time of maximum in units of solar longitude. The time of maximum, duration of the shower (degrees), geocentric radiant coordinates (J2000.0) and velocity at the time of maximum together with the radiant drift and associated error are shown. Note that drifts are not computed for showers with 3 days duration. The raw wavelet coefficient at the time of maximum and the number of standard deviations that this value is above the median background is also given; the latter is a better indicator of absolute relative activity between streams. The 62 new showers found in this survey are shown with an asterisk (*) after the IAU code.

IAU name	IAU code	λ_{max}	λ_{start}	λ_{end}	Dur.	α_g	δ_g	$\Delta\alpha$	$\pm(\Delta\alpha)$	$\Delta\delta$	$\pm(\Delta\delta)$	W_{Cmax}	σ_{wave}	V_g
Daytime April Piscids	APS	26	16	38	23	4.9	5.5	0.94	0.02	0.42	0.02	569.4	8.6	29.2
April Lyrids	LYR	32	30	34	5	272.2	32.6	0.62	0.18	−0.33	0.13	492.3	32.8	46.6
Beta Pegasids	BPG*	36	24	49	26	350.5	27.8	0.63	0.04	0.34	0.03	151	7.1	41
April rho Cygnids	ARC*	37	34	43	10	324.5	45.9	0.61	0.05	0.36	0.04	317.7	20.5	41.8
Lambda Lyrids	LLY*	41	32	54	23	283.7	28.5	0.72	0.04	−0.15	0.02	430.5	42.1	33.4
May Lacertids	MAL*	42	42	48	7	335.6	45.3	0.61	0.42	0.5	0.25	212.3	12.2	43
Eta Aquariids	ETA	45	30	66	37	337.9	−0.9	0.7	0.01	0.33	0	4100	257.4	63.6
Daytime Triangulids	DTR*	46	44	46	3	35.9	34.1	0	0	0	0	46.8	5.3	26.2
Zeta Ophiuchuids	ZOP*	47	44	48	5	254.8	−4.4	0.74	0.19	−0.29	0.29	46	4.4	22.8
Northern Daytime omega-Cetids	NOC	49	16	61	46	11.8	18.9	0.99	0.01	0.36	0.01	1006	38.4	36.2
Sigma Cetids	SCT*	49	49	51	3	39	−15.7	0	0	0	0	26.7	6.2	35.5
Southern Daytime omega-Cetids	OCE	49	11	65	55	23.4	−4.3	0.91	0	0.46	0	1081	76.3	37
Daytime Delta Triangulids	DDT*	53	52	56	5	35.3	33.7	1.95	0.17	0.91	0.17	86.4	8.1	28.4
Daytime xi_2 Cetids	XIC*	54	54	57	4	36.4	8.6	1	0.14	0.3	0.8	63	11.6	16.5
Epsilon Aquilids	EAU	54	51	55	5	278.7	13.4	1.1	0.39	0.23	0.31	190	21.3	31.4
May Vulpeculids	MVL*	54	54	82	29	287.2	22.5	0.66	0.29	−0.09	0.26	219.8	26.9	32.5
Phi Pegasids	PHP*	54	51	55	5	358.3	20.7	0.72	0.17	−0.01	0.29	89.6	9.5	30.4
South Daytime May Arietids	SMA	54	36	59	24	36.3	10.8	0.96	0.01	0.3	0.01	796.3	34.2	28
Tau Ophiuchuids	TOP*	55	54	57	4	269.3	−6.4	0.03	0.1	−0.55	0.26	104.7	7	37
August zeta Cygnids	ECY*	60	59	61	3	318.2	29.8	0	0	0	0	52.8	6.2	29.2
Psi Pegasids	PSP*	63	61	65	5	1.8	28.1	1.11	0.17	0.7	0.27	45.9	5.1	30.8
Theta Serpentids	TSR*	65	60	74	15	284	6	0.77	0.04	−0.35	0.07	167.2	17.1	32
Daytime zeta Perseids	ZPE	74	56	90	35	56.6	23.2	0.99	0.01	0.23	0.01	620	21.6	27.1
June Mu Cassiopeids	JMC*	74	49	95	47	17.5	53.9	0.91	0.08	0.28	0.07	226.6	16.6	43.6
Southern June Aquilids	SZC	80	79	83	5	305.3	−33.2	0.24	0.11	0.16	0.1	539.1	45.7	37.7
Daytime Arietids	ARI	81	62	99	38	45.7	25	0.86	0.03	0.18	0.01	3384	125.2	39.1
Daytime lambda Taurids	DLT	86	71	98	28	57.3	11.4	0.85	0.01	0.33	0.01	471.9	13.4	35.6
Zeta Eridanids	ZER*	93	93	97	5	50.8	−4.1	0.64	0.1	0.44	0.27	40.1	6.8	50.9
Daytime beta Taurids	BTA	94	89	101	13	82.8	20.1	0.82	0.05	0.05	0.02	553.1	14.1	26.8
Kappa Cetids	KCT*	94	94	98	5	51	4.6	1.71	0.2	0.95	0.11	63	7.4	29.2
Epsilon Perseids	EPE	96	91	107	17	58.3	37.5	0.87	0.03	0.14	0.02	239.3	10.4	44.6
Beta Camelopardalids	BCM*	100	99	112	14	59.7	59.7	2.1	0.1	0.03	0.04	119.5	7.8	42.7
July beta Pegasids	JBP*	100	99	101	3	349.1	34.4	0	0	0	0	48.3	7.7	27.8
Omicron Pegasids	OPG*	100	99	101	3	336.9	31.2	0	0	0	0	65.1	8.6	28.5
July Andromedids	JAD*	101	97	101	5	36.1	49.1	0.68	0.5	0.96	0.25	80.4	9.8	34.7
Northern June Aquilids	NZC	101	71	123	53	310.4	−4.2	0.845	0.01	0.182	0.01	846.9	44.9	37.5
July Taurids	JTR*	104	95	112	18	70	1.5	0.81	0.06	0.16	0.1	94.1	14	39.7
Microscopiids	MIC*	104	90	115	26	320.3	−28.3	0.89	0.01	0.29	0.01	310.1	8	38
Epsilon Pegasids	EPG	105	97	105	9	324.3	13.2	1.15	0.09	−0.3	0.14	412.8	40.9	30.3
Alpha Pegasids	APG*	106	105	107	3	353.9	17.8	0	0	0	0	33.1	7.3	35.9
Phi Piscids	PPS*	106	104	107	4	20.1	24.1	1.56	0.45	0.36	0.16	207.2	4.7	62.9
Theta Perseids	TPR*	106	105	110	6	41.1	47.6	0.87	0.09	−0.07	0.09	70.3	10	53
Beta Equuleids	BEQ	107	106	118	13	322.8	8.2	0.71	0.05	−0.28	0.07	468.5	36	31.2
Alpha Lacertids	ALA	109	100	115	16	348	51.6	1.1	0.06	0.42	0.02	327.6	18.2	38.3
Psi Cassiopeids	PCA	120	100	129	30	14.8	66.6	0.96	0.09	0.38	0.02	1033	45.6	44.8
Alpha Capricornids	CAP	123	108	140	33	303.1	−10.7	0.6	0.01	0.3	0.02	648.5	24.4	22
Southern delta Aquariids	SDA	126	114	164	51	340.8	−16.3	0.78	0	0.3	0.01	7800	177.7	40.7
Iota Sculptorids	ISC*	128	126	129	4	5.2	−28.1	0.23	0.27	−0.4	0.27	44.7	8.5	36.7
August omicron Eridanids	OME*	134	132	136	5	66.9	−8.3	1.22	0.27	0.08	0.4	17.6	4.7	45
August Lyncids	ALN*	135	116	136	21	119.8	55.1	1.52	0.1	−0.23	0.04	93.1	6.3	41.7
Piscis Austrinids	PAU	135	124	142	19	357.1	−21.5	0.52	0.05	0.39	0.04	218.6	14.8	44
Delta Monocerotids	DMO*	137	136	138	3	114.1	−3.1	0	0	0	0	34.5	8.2	37.2
Daytime xi Orionids	XRI	137	128	140	13	107.5	16.2	0.7	0.04	−0.1	0.03	241.8	11.8	43.8
Gamma Eridanids	GER*	138	138	140	3	61.9	−17.4	0	0	0	0	51.1	5	56.9
Northern delta Aquariids	NDA	139	126	156	31	345.7	2.3	0.72	0.01	0.26	0.01	554.3	12.6	37.3
Perseids	PER	140	123	147	25	48	57.2	1.39	0.02	0.29	0.01	1200	90.7	61.4
Southern iota Aquariids	SIA	140	133	144	12	340.2	−11.4	0.87	0.04	0.41	0.04	313.9	4.6	29.1
August Cetids	ACT*	153	153	156	4	7	−5.6	1.85	0.26	0	0	55.3	7	20.2
Kappa Draconids	KDR*	158	155	161	7	189.4	73.1	0.95	0.69	−0.7	0.15	79.8	8.2	38
Northern iota Aquariids	NIA	159	145	164	20	355.4	3.4	0.84	0.01	0.39	0.01	572.8	7.5	28.7
Daytime zeta Cancrids	ZCA	160	140	167	28	136.1	11.7	0.92	0.02	−0.18	0.01	301.7	16.6	42.1
Daytime pi Leonids	DPL*	174	172	182	11	145.6	8.7	0.76	0.14	−0.34	0.06	228.2	4.6	41.7
Daytime kappa Leonids	KLE	183	164	200	37	162.3	14.9	0.62	0.01	−0.3	0.01	592.9	21	43.3
Beta Ursae Majorids	BUM*	184	183	187	5	161.2	56.5	1.53	0.59	0.1	0.13	76.7	6.8	50.3
Daytime Sextantids	DSX	186	174	197	24	154.3	−1	0.56	0.04	−0.54	0.02	1408	89.3	31.3
Lambda Draconids	LDR*	196	195	212	18	156.1	74.7	1.29	0.1	−0.23	0.06	155	10.6	37.5
Southern Taurids	STA	196	173	217	45	30.9	8.1	0.817	0.005	0.291	0.004	1479	29.9	28.2
October eta Eridanids	OEE	201	200	202	3	45.8	−9.8	0	0	0	0	37.1	7.8	25.4
October Ursae Majorids	OCU	202	201	203	3	143.8	63.9	0	0	0	0	193.7	13.5	58.1

Table 1 (*continued*)

IAU name	IAU code	λ_{max}	λ_{start}	λ_{end}	Dur.	α_g	δ_g	$\Delta\alpha$	$\pm(\Delta\alpha)$	$\Delta\delta$	$\pm(\Delta\delta)$	W_{Cmax}	σ_{wave}	V_g
October Leporids	OLP*	203	196	206	11	81.6	−13.8	1.08	0.14	0.26	0.06	173.6	70	25.5
Orionids	ORI	208	198	227	30	95.5	15.2	0.78	0.01	0.02	0.01	2507	82.5	65.4
Alpha Ursae Majorids	AUM*	209	198	214	17	174.6	64.6	1.07	0.11	−0.55	0.11	164.5	19.1	35.6
Leonis Minorids	LMI	210	199	213	15	160.7	35.7	1.22	0.07	−0.4	0.05	182.8	13.7	59.8
Xi Draconids	XDR	211	209	215	7	171.2	70.6	0.98	0.25	−0.63	0.19	236.1	8.3	37.1
October beta Camelopardalids	OBC*	214	200	215	16	66.8	56.2	1.45	0.09	0.3	0.07	77.2	8.1	47.6
October kappa Draconids	OKD*	216	215	224	10	182.1	63.4	0.95	0.14	−0.47	0.22	239.6	16.8	37.3
Northern Taurids	NTA	219	217	241	25	48.9	17.7	0.84	0.01	0.25	0.02	776.5	13.4	28.1
Chi Taurids	CTA*	220	194	227	34	63.2	24.7	0.96	0.01	0.19	0.01	440.6	8.2	42.1
Omicron Eridanids	OER	227	213	243	31	55.6	−1.5	0.74	0.48	0.64	0.21	66.5	5.9	26.1
Omega Eridanids	OME*	234	232	235	4	73.3	−5.3	0.95	0.05	0.35	0.26	49.4	8.6	31.8
Leonids	LEO	237	230	237	8	155.1	21.1	0.55	0.06	−0.37	0.2	523.7	20.1	67.3
November theta Aurigids	THA*	237	233	239	7	89	34.7	1.49	0.13	0.14	0.14	226.6	11	33.8
November delta Draconids	NDD*	241	240	242	3	277.7	68.2	0	0	0	0	81.6	6	25.5
Gamma Taurids	GTA	241	240	242	3	68.1	13	0	0	0	0	48.3	6.9	15.7
November I Draconids	NID*	241	221	264	44	200.1	64.5	0.72	0.11	−0.31	0.08	606.1	18.1	43
Rho Bootids	RBO*	242	241	243	3	215.7	31.8	0	0	0	0	131.3	5.3	43
November omega Orionids	NOO	246	225	256	32	90.5	15.3	0.761	0.01	−0.04	0.01	1704	83.2	43.1
Alpha Canis Majorids	ACA*	247	247	265	19	100.2	−17.3	0.69	0.09	0.44	0.06	87.6	36.3	42
Gamma Canis Majorids	GCM*	257	255	258	4	109.8	−11.3	0.43	0.23	−0.17	0.11	83.1	6.7	43.6
Sigma Hydrids	HYD	258	251	267	17	127.7	2.5	0.96	0.02	−0.26	0.03	117.3	11.8	59.2
December theta Aurigids	DTA*	261	261	263	3	93	36.6	0	0	0	0	58.9	11.1	58.9
December Monocerotids	MON	261	257	266	10	102.3	8.6	0.69	0.02	−0.24	0.08	499.7	38.1	40.6
Geminids	GEM	261	240	273	34	112.5	32.1	1.12	0.01	−0.17	0.01	16476	278.3	34.5
Nu Geminids	NGM*	262	261	263	3	99	18.1	0	0	0	0	8.3	7.9	65.8
December Canis Majorids	DCM*	266	264	266	3	112.3	−14.6	0	0	0	0	140.7	50.3	42.8
December Hydrids	DHY*	266	261	281	21	131.5	−11.3	0.89	0.02	−0.58	0.02	77.3	18.4	54.5
December Leonis Minorids	DLM	268	261	286	26	162.2	29.9	0.91	0.02	−0.47	0.02	180.8	11.1	62.8
Ursids	URS	270	269	272	4	222.1	74.8	1.77	0.46	−0.05	0.38	494.8	34.8	35.6
Beta Monocerotids	BMO*	271	271	273	3	100.5	−8.8	0	0	0	0	39.9	8	31
Sigma Serpentids	SSE	275	255	291	37	242.4	−0.1	0.64	0.02	0.03	0.02	604.6	22.2	42.3
January Leonids	JLE	282	279	287	9	148.2	23.7	0.7	0.03	−0.13	0.03	760.1	111.9	52.3
Kappa Hydrids	KHY	283	281	283	3	139.1	−12.9	0	0	0	0	38.3	6.8	37.6
Quadrantids	QUA	283	232	291	60	231.5	48.5	0.78	0.01	−0.38	0.01	7644	141.9	41.7
Alpha Hydrids	AHY	286	267	300	34	128.5	−8.6	0.64	0.01	−0.12	0.03	339.9	32.8	43.2
Daytime xi Sagittariids	XSA	288	278	296	19	282.3	−16.3	0.77	0.02	0.12	0.02	352.3	12.8	25.3
Beta Sextantids	BSX*	292	286	293	8	160.2	1.8	1.15	0.13	−0.44	0.09	80.5	4.5	53.2
January Hydrids	JHY*	292	281	294	14	149.7	−22.1	1.14	0.1	−0.83	0.1	64	12	37.9
Canum Venaticids	CVN*	293	291	296	6	203.3	42.8	0.33	0.2	−0.3	0.39	69.3	9	52.6
Xi Coronae Borealids	XCB	295	287	304	18	247	30.3	0.39	0.04	0.11	0.02	559.2	35.3	44.8
Lambda Bootids	LBO	296	280	297	18	221.5	42.4	1.04	0.05	−0.76	0.02	817.1	41.9	40.7
Theta Coronae Borealids	TCB	296	287	304	18	233.6	34.4	0.3	0.08	0.16	0.05	934.6	35.1	37.7
Gamma Ursae Minorids	GUM*	299	294	304	11	231.8	66.8	0.7	0.1	−0.57	0.09	233.9	13.2	31.8
Mu Hydrids	MHY*	300	299	306	8	154.3	−20.9	0.65	0.13	0.76	0.26	136.6	23.8	39.1
Daytime chi Capricornids	DCS	301	294	315	22	304.7	−29.2	0.73	0.04	0.24	0.04	213.4	12.9	23.8
Alpha Antliids	AAN	312	295	332	38	160.7	−12.3	0.745	0.02	−0.36	0.01	793.4	62.3	43.2
February Comae Beriniciids	FCB*	324	323	325	3	186.2	29.1	0	0	0	0	32.9	5	24.2
Daytime kappa Aquariids	MKA*	350	346	350	5	332	−8.4	1.75	0.3	0.39	0.19	262.5	3.7	31.4

and argument of perihelion under differential secular precession (Babadzhanov and Obrubov, 1992). More evolved streams may also intersect the Earth at more than one location (in fact up to eight intersections are possible from one initial stream under the action of planetary perturbations). In cases where evolution of an initial stream (usually with low inclination) produces showers visible at the ascending and descending node, we refer to the streams as north (descending node) and south (ascending) nodal branches. Usually, stream activity for the branches occurs at the same time of the year and radiants are symmetric about the ecliptic plane. For common stream intersections pre-perihelion and post-perihelion we refer to the streams as twin showers following Whipple (1940); for prograde streams one shower in such twin streams is a nighttime shower and the other a Daytime shower and both typically have similar orbital elements, but differing values of Ω and ω. Details of the underlying dynamics can be found in discussions by Babadzhanov and Obrubov (1992) and Sekanina (1973). We note that particularly twin associations in our data may be somewhat uncertain as the mean stream elements are affected by observational error.

5.1. Stream complexes

For evolved streams, linkages with parent objects or other streams is more complex. We shall argue that some of our showers are part of broader complexes reflecting an intermediate stage of evolution for showers merging into the sporadic background, where evolved streamlets are still detectable, but direct orbital linkage with parents is no longer possible.

The "arc" of stream radiant maxima seen in Fig. 3 follows nearly the same radiant pattern as a feature of sporadic radiants first reported by Campbell-Brown (2008) as part of a separate examination of sporadic meteor radiants measured by CMOR. The "ring" structure found in that study was located about 55° away from the apex direction, was approximately 10° in width, and in the high number statistics used for the sporadic study, it completely surrounds the apex direction. The "ring" feature varies in visibility throughout the year, reflecting changes in strength. The sporadic ring was manifested as both a relative increase in radiant densities and in a marked difference in orbital elements for the population of meteoroids having radiants along the ring relative to those in sur-

Table 2
For all the showers from Table 1, mean orbits are computed using the radiant and velocity observed at the time of maximum. The standard orbital elements are given with a (semi-major axis), q (perihelion) in AU, while inclination (i), argument of perihelion (ω) and argument of the ascending node (Ω) are in degrees referenced to J2000.0. N_{orb} refers to the number of orbits used to compute the wavelet coefficient at the time of maximum and hence is a measure of the number of orbits being used to compute the mean stream orbit.

IAU code	λ_{max}	a	e	q	i	ω	Ω	N_{orb}
APS	26	1.53	0.837	0.2493	4.5	49.49	26.0	2608
LYR	32	10.85	0.916	0.9149	80.0	215.71	32.0	1197
BPG	36	2.76	0.890	0.3036	62.7	61.11	36.0	1105
ARC	37	6.51	0.875	0.8099	69.9	125.55	37.0	1006
LLY	41	0.95	0.261	0.7033	68.9	297.35	41.0	1256
MAL	42	11.14	0.935	0.7249	70.6	114.76	42.0	881
ETA	45	4.14	0.874	0.5232	162.9	88.15	45.0	3274
DTR	46	4.24	0.868	0.5613	16.2	92.58	46.0	519
ZOP	47	0.92	0.674	0.2997	19.9	318.22	47.0	567
NOC	49	1.44	0.919	0.1167	34.8	32.13	49.0	2279
SCT	49	5.21	0.920	0.4170	41.1	257.00	229.0	400
OCE	49	1.70	0.924	0.1282	34.8	215.17	229.0	2205
DDT	53	2.95	0.847	0.4523	19.6	78.17	53.0	823
XIC	54	1.00	0.546	0.4538	3.7	235.95	234.0	709
EAU	54	0.89	0.624	0.3356	59.2	317.61	54.0	991
MVL	54	0.88	0.446	0.4900	66.9	312.18	54.0	1270
PHP	54	0.75	0.854	0.1096	50.1	20.68	54.0	1086
SMA	54	1.61	0.817	0.2957	4.4	235.01	234.0	3289
TOP	55	1.24	0.898	0.1264	48.7	328.11	55.0	892
ECY	60	0.69	0.467	0.3691	67.7	4.16	60.0	446
PSP	63	0.76	0.800	0.1512	57.7	23.88	63.0	357
TSR	65	0.93	0.745	0.2368	54.3	322.68	65.0	625
ZPE	74	1.65	0.800	0.3305	3.9	58.84	74.0	2304
JMC	74	57.24	0.990	0.5773	68.3	97.68	74.0	584
SZC	80	1.04	0.936	0.0659	56.1	159.00	260.0	426
ARI	81	1.75	0.961	0.0692	28.0	25.57	81.0	3592
DLT	86	1.50	0.925	0.1123	22.6	211.69	266.0	2059
ZER	93	3.22	0.928	0.2301	103.5	232.64	273.0	390
BTA	94	1.94	0.802	0.3833	3.5	246.47	274.0	1386
KCT	94	0.75	0.886	0.0850	35.7	198.05	274.0	523
EPE	96	4.15	0.970	0.1263	62.3	38.83	96.0	1139
BCM	100	67.75	0.993	0.5083	63.7	89.78	100.0	507
JBP	100	0.62	0.651	0.2155	67.4	357.06	100.0	396
OPG	100	0.66	0.605	0.2616	66.0	345.97	100.0	470
JAD	101	0.89	0.693	0.2748	69.7	38.44	101.0	615
NZC	101	1.55	0.925	0.1160	39.5	327.49	101.0	1689
JTR	104	1.54	0.900	0.1548	60.9	217.82	284.0	513
MIC	104	1.68	0.935	0.1088	36.7	147.95	284.0	739
EPG	105	0.79	0.780	0.1733	54.2	333.27	105.0	1271
APG	106	0.58	0.841	0.0925	107.7	352.04	106.0	441
PPS	106	2.09	0.590	0.8559	152.6	125.02	106.0	1395
TPR	106	4.53	0.898	0.4617	104.4	81.16	106.0	657
BEQ	107	0.86	0.824	0.1517	48.3	331.99	107.0	1588
ALA	109	1.04	0.033	1.0087	80.6	221.08	109.0	1163
PCA	120	2.48	0.622	0.9378	83.4	143.06	120.0	1875
CAP	123	2.26	0.742	0.5836	6.7	269.93	123.0	740
SDA	126	2.20	0.970	0.0657	30.6	154.08	306.0	4819
ISC	128	1.02	0.788	0.2158	69.1	141.83	308.0	336
OER	134	0.86	0.504	0.4250	108.7	222.87	314.0	444
ALN	135	32.65	0.987	0.4383	57.6	81.76	135.0	443
PAU	135	3.10	0.955	0.1395	65.6	139.96	315.0	1637
DMO	137	4.11	0.920	0.3274	41.1	245.62	317.0	377
XRI	137	3.24	0.986	0.0461	32.2	202.67	317.0	1089
GER	138	3.15	0.686	0.9870	113.9	339.34	318.0	493
NDA	139	1.70	0.944	0.0955	23.4	329.94	139.0	2096
PER	140	−9.91	1.096	0.9560	115.6	153.12	140.0	2024
SIA	140	1.65	0.836	0.2709	4.0	127.51	320.0	2209
ACT	153	0.82	0.692	0.2537	8.3	146.20	333.0	355
KDR	158	−10.53	1.085	0.8989	57.5	142.16	158.0	363
NIA	159	1.57	0.827	0.2705	6.9	308.07	159.0	1891
ZCA	160	4.64	0.981	0.0883	16.6	212.57	340.0	949
DPL	174	2.35	0.975	0.0585	20.2	204.80	354.0	1110
KLE	183	6.79	0.987	0.0911	24.1	33.84	183.0	1366
BUM	184	−26.45	1.026	0.6868	85.0	112.24	184.0	565
DSX	186	1.07	0.858	0.1511	22.0	212.99	6.0	1292
LDR	196	1.33	0.264	0.9759	72.5	152.87	196.0	1337
STA	196	1.72	0.820	0.3084	5.3	122.26	16.0	2497
OEE	201	1.33	0.688	0.4140	26.4	115.82	21.0	375
OCU	202	−8.55	1.115	0.9810	103.3	165.74	202.0	1223
OLP	203	0.71	0.610	0.2780	50.0	154.59	23.0	380
ORI	208	5.47	0.895	0.5746	162.8	83.98	28.0	2536
AUM	209	1.10	0.213	0.8665	70.5	105.32	209.0	1237
LMI	210	4.63	0.875	0.5782	124.7	95.88	210.0	676
XDR	211	1.28	0.231	0.9858	71.9	162.33	211.0	1363
OBC	214	6.57	0.936	0.4174	80.9	281.50	214.0	355
OKD	216	1.26	0.267	0.9208	72.2	130.83	216.0	1307
NTA	219	2.06	0.830	0.3508	0.4	115.09	39.1	2281
CTA	220	4.97	0.984	0.0807	12.3	328.49	220.0	1850
OER	227	2.63	0.803	0.5176	18.4	94.11	47.0	623
OME	234	2.49	0.833	0.4174	34.1	105.79	54.0	431
LEO	237	2.52	0.610	0.9838	162.0	171.11	237.0	2268
THA	237	1.13	0.897	0.1160	27.8	330.07	237.0	1180
NDD	241	4.61	0.786	0.9856	39.5	185.41	241.0	536
GTA	241	1.18	0.507	0.5825	4.9	102.63	61.0	426
NID	241	3.76	0.737	0.9874	74.9	181.09	241.0	2059
RBO	242	2.64	0.781	0.5774	73.0	93.07	242.0	606
NOO	246	12.01	0.991	0.1066	26.0	142.37	66.0	1923
ACA	247	3.70	0.862	0.5114	67.1	92.32	67.0	338
GCM	257	3.13	0.881	0.3732	70.2	109.05	77.0	429
HYD	258	14.43	0.982	0.2578	131.3	119.33	78.0	604
DTA	261	−0.46	1.504	0.2339	35.5	285.63	261.0	1208
MON	261	8.88	0.978	0.1936	32.4	128.65	81.0	1598
GEM	261	1.35	0.898	0.1373	23.2	324.95	261.0	10381
NGM	262	−0.38	1.217	0.0825	26.7	132.01	82.0	545
DCM	266	7.04	0.937	0.4434	63.7	97.80	86.0	558
DHY	266	4.82	0.915	0.4073	105.9	103.08	86.0	602
DLM	268	6.73	0.916	0.5662	135.5	263.57	268.0	1304
URS	270	24.11	0.961	0.9470	55.5	202.53	270.0	1021
BMO	271	3.84	0.863	0.5264	33.0	90.20	91.0	363
SSE	275	1.90	0.916	0.1596	62.4	41.20	275.0	1075
JLE	282	5.34	0.990	0.0517	107.9	334.71	282.0	1160
KHY	283	1.04	0.793	0.2149	66.5	140.08	103.0	621
QUA	283	3.35	0.709	0.9746	72.4	168.14	283.0	6614
AHY	286	8.62	0.966	0.2910	57.0	115.64	106.0	770
XSA	288	2.18	0.784	0.4708	6.0	79.31	288.0	896
BSX	292	1.84	0.962	0.0694	149.7	153.55	112.0	595
JHY	292	0.97	0.708	0.2826	73.0	136.00	112.0	316
CVN	293	9.40	0.908	0.8659	93.3	221.54	293.0	1105
XCB	295	2.84	0.718	0.8007	79.3	123.70	295.0	2621
LBO	296	1.36	0.291	0.9647	78.3	203.90	296.0	2743
TCB	296	1.04	0.172	0.8601	76.0	98.20	296.0	3560
GUM	299	4.20	0.772	0.9593	51.1	199.54	299.0	694
MHY	300	1.08	0.770	0.2489	71.8	135.79	120.0	497
DCS	301	2.67	0.792	0.5559	7.3	270.86	121.0	428
AAN	312	1.94	0.929	0.1367	64.3	141.99	132.0	1228
FCB	324	0.95	0.620	0.3619	30.5	310.97	324.0	330
MKA	350	1.83	0.872	0.2339	4.6	50.12	350.0	1457

rounding regions (cf. Campbell-Brown, 2008). In particular, the inner edge of the ring shows a noticeable dip in radiant density. Campbell-Brown (2008) ascribed the depleted number of radiants in the inner part of the ring to a higher collisional probability for meteoroids with radiants in the ring (such particles having a ~1 AU). More recently, Wiegert et al. (2009) have suggested that the ring structure is an expected consequence of the Kozai resonance for meteoroids with small ($a \sim 1$–2 AU) semi-major axis which are spiraling inward under the Poynting–Robertson effect.

To investigate possible linkages among our streams, we have performed two quantitative comparisons, one using orbital secular invariants and the other the standard orbital D'-criterion (Drummond, 1981).

The first approach is to use the orbital secular invariants proposed by Valsecchi et al. (1999) that include the velocity of the meteoroid when it collides with the Earth in units of Earth's orbital velocity, U, a value related to the Tisserand invariant (relative to the Earth) as $U = (3 - T)^{1/2}$. The other variable is the angle between the geocentric radiant and the apex direction of the Earth's motion, Θ.

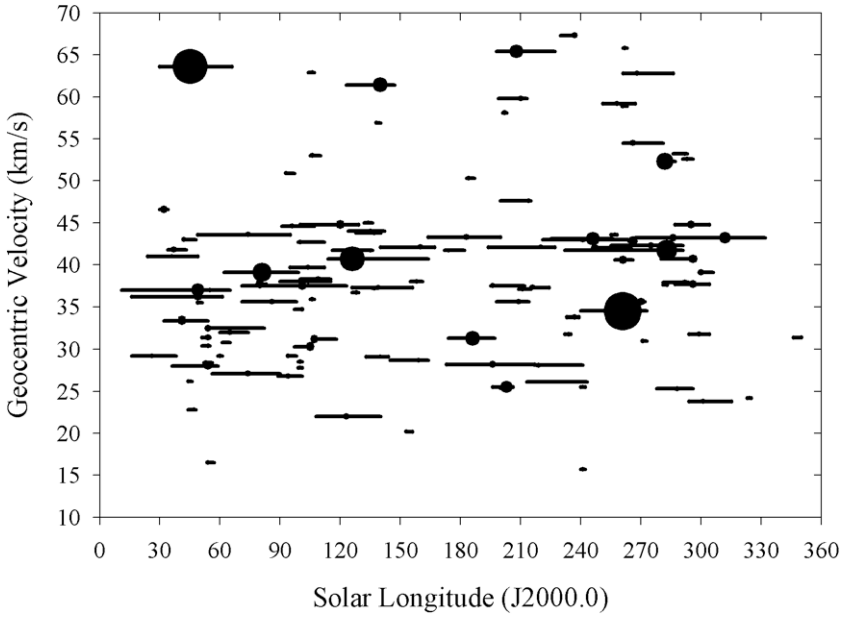

Fig. 2. The distribution throughout the year and as a function of geocentric velocity for all 117 streams found in our survey. The horizontal lines delineate the time period where each shower is active. The circle denotes the time of maximum and the size of the circle is linearly proportional to the strength of the shower.

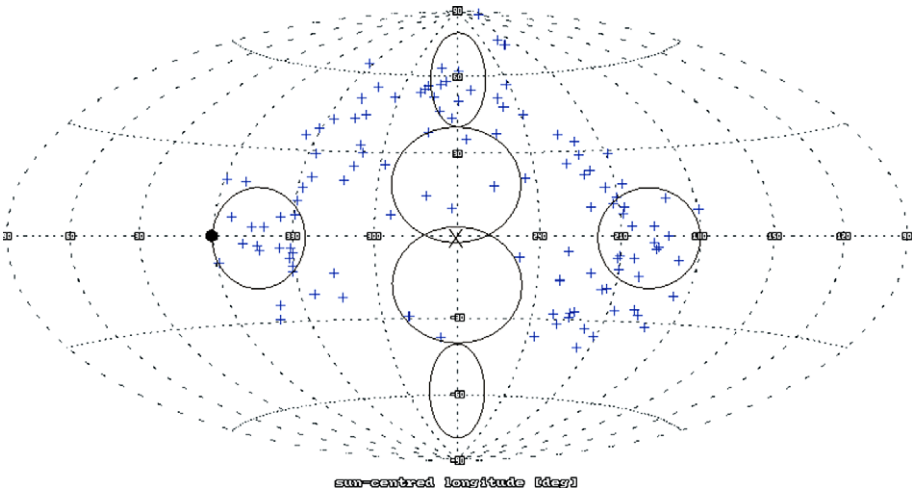

Fig. 3. The radiant location for all showers shown in sun-centered coordinates. The circles represent the approximate locations and extents of the major sporadic sources as given in Jones and Brown (1993). The Sun is shown by a dark circle at the origin; the center of the plot (marked with an *X*) is the apex of the Earth's way.

In practice, cos Θ is used because it depends linearly on orbital energy (also a quasi-constant of motion). As shown by Valsecchi et al. (1999) and Jopek et al. (1999), meteoroids starting from a common orbit and evolving purely under gravitational perturbations have values of (U, cos Θ) which are similar. Because these quantities are linked to secular invariants, recently evolved meteoroids starting from a common stream will have similar (U, cos Θ). Here we use the mean stream orbits to examine possible interstream linkages. We emphasize that common values of (U, cos Θ) are a necessary but not sufficient condition to establish that two separate streams are evolved components of a common parent. To establish more rigorously interstream links requires following numerically the evolution of stream orbits over long periods, including the effects of radiation forces, a process beyond the scope of this work.

Fig. 4 shows the locations of all our mean stream orbits in a cos Θ vs. U plot. Here the upper line corresponds to hyperbolic orbits intersecting the Earth's orbit; those below the lower solid line are Aten-like orbits which are mostly interior to the Earth's orbit. Fig. 5 is the same plot but for all comets and near-Earth asteroids whose orbits get closer than 0.05 AU to the Earth. Most of our showers are located in the portion of the diagram proximal to nearly isotropic comets (NIC) and Halley-type comets (HTC). There are a few showers located on the periphery of the near-Earth asteroid (NEA)/Jupiter-Family comet (JFC) portion of the diagram. The two showers where a linkage with NEAs is most probable are the Gamma Taurids (GTA) and newly identified Daytime xi_2 Cetids (XIC). Both showers are strongly above background during their time of activity, leaving little question that they are real showers. We find no linkage with a specific NEA in either case, not unsurprising given the fast evolution of shower meteoroids in such small orbits.

In Fig. 6 we show the expected magnitude and timescales of spread for meteoroids released from different classes of parent bodies. Here our simulated meteoroids have masses of $\sim 10^{-8}$ kg, representative of our survey population, and the simulation proceeds for 50,000 years. The simulations were run with a symplectic

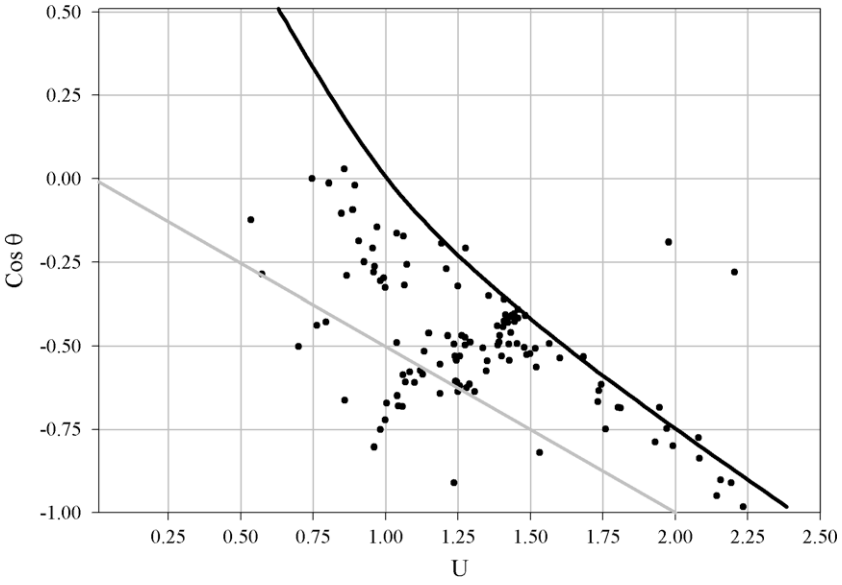

Fig. 4. All showers detected by our survey plotted as a function of U and cos Θ (for definitions of these quantities see text and Valsecchi et al. (1999)). The upper solid line is the cutoff for Earth-intersecting parabolic orbits (orbits above this line are unbound with respect to the Sun) while the lower line represents objects on Aten-like orbits (where $a < 1$ AU).

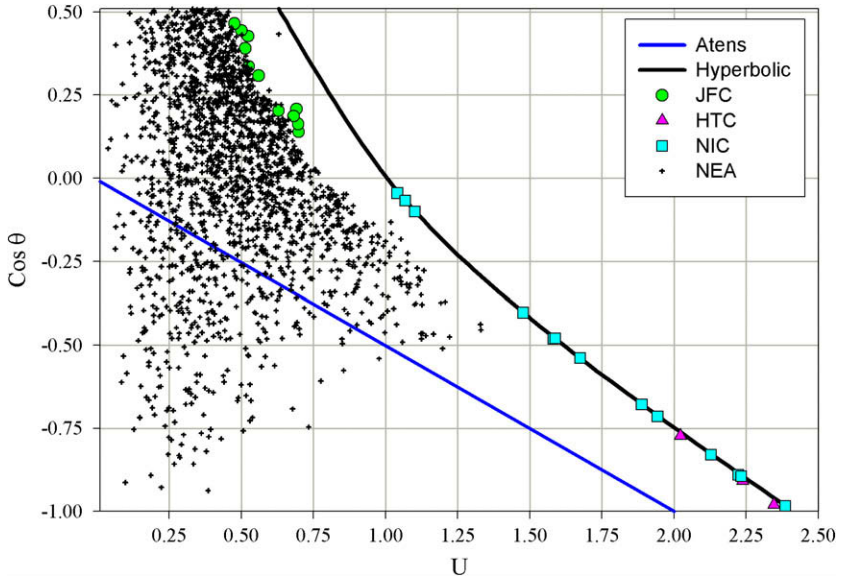

Fig. 5. The same plot as Fig. 4 but for all comets and asteroids with orbital intersections with the Earth less than 0.05 AU. The populations are distinct with the longer period comets (including nearly isotopic (NIC) comet and Halley-type comets (HTCs) using the classification system proposed by Levison (1996)) lying on the parabolic line and JFCs shifted to lower intersection velocities with some overlap with the NEA population. Data for cometary orbits are from Green (2008) while those for near Earth objects are from the NeoDys website (http://newton.dm.unipi.it/neodys/, downloaded April 28, 2009).

numerical integration code (Wisdom and Holman, 1991) that handles close encounters by the Chambers hybrid method (Chambers, 1999). Poynting–Robertson drag was included and the particles beta (defined as the ratio of the reflected sunlight force to gravitational force on the particle) assumed to be 4e−3, corresponding to a few hundred micron diameter particle. Note that the meteoroids are plotted only when their orbits are within 0.05 AU of the Earth; U and cos Θ are undefined for non-intersecting orbits. As expected, objects on higher inclination orbits show very slow evolution away from their parent. For NIC and HTCs, the variation of U, cos Θ with time is typically so small that links with parent objects should be possible over many tens of ka. What evolution does occur, relative to the parent body, tends to be parallel and close to the parabolic limit line. For meteoroids with JFC parents, we find that the ejected population spreads along a line parallel to the parabolic limit line and in some cases ultimately (after of order 10 ka depending on the starting orbit) the meteoroid orbits shrink sufficiently under the Poynting–Robertson effect that they move down into the Aten-orbit region.

It is difficult to generalize the timescales as they depend on the parent starting orbit, but it does suggest that our Aten-like and more evolved showers can potentially be best explained as having evolved from JFCs in this general way. Typical NEA starting orbits produce particles which evolve nearly perpendicular to the Aten line; however the specifics depend on the starting orbit and for some of our showers NEA parents certainly cannot be ruled out.

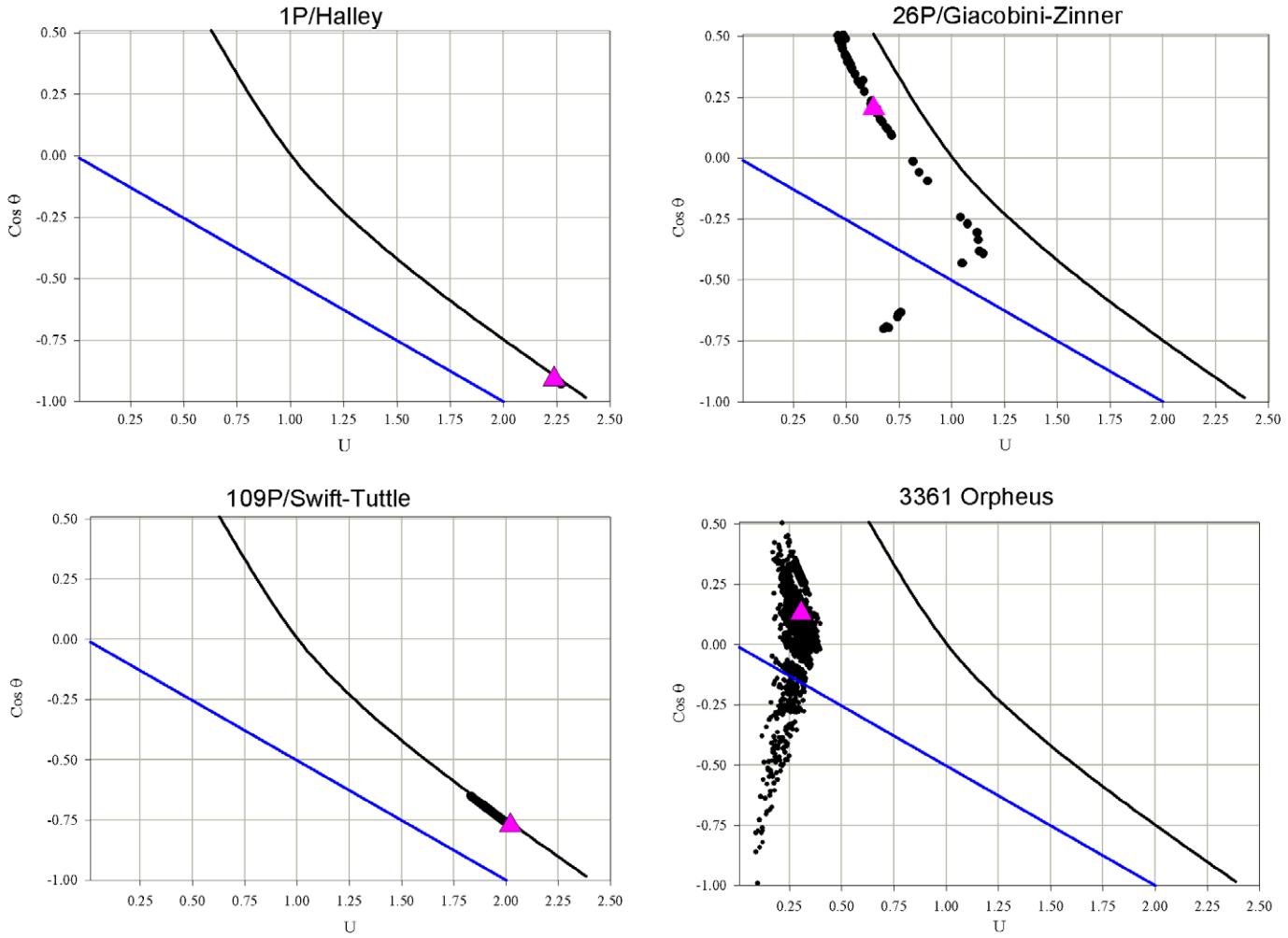

Fig. 6. Evolutionary paths for meteoroids with mass of 10^{-8} kg starting from four representative parent body orbits. A total of 20 test particles are ejected from the starting orbit of each parent and integrated forward in time to demonstrate general evolutionary behavior in U, cos Θ. Only particles whose orbits intersected the Earth within 0.05 AU at any particular epoch are shown. The integrations continue for 50 ka in the plots – the parent (starting) orbits are shown as enlarged triangle symbols in each plot and the specific parent chosen for the example is given in each graph. Note that the particles farthest from the starting orbit are typically the oldest. Upper left (1P/Halley) represents the Halley-type comets, upper right (26P/Giacobini–Zinner) represents Jupiter-Family comets, lower left (109P/Swift–Tuttle) represents another example of a longer period Halley-type comet (closer to being a nearly isotropic – returning comet than 1P/Halley) and (bottom right) 3361 Orpheus is a near-Earth asteroid.

Linkages with the original parent, for either NEAs or JFCs, would no longer be possible after less than 10 ka in most cases.

To search for potential stream linkages, we first estimate the error in our position for (U, cos Θ) based on a presumed mean error of 5% in measured mean stream velocity and 2° in radiant location at the time of peak. We then select multiple showers as potentially linked if their values of (U and cos Θ) overlap within error and if they are separable from other shower concentrations. The results of this procedure are a series of seven possible "complexes" which we name based on the member shower showing the highest activity in our data. By definition these complexes would be necessarily young (based on the timescale of the spread in U and cos Θ in our simulations). Table 3 shows the stream "complexes" linked in this way.

Among these complexes, the LLY, SZC and SDA complexes have radiant distributions overlapping the sporadic "ring" feature discussed earlier and shown in Fig. 7. Indeed, it appears that the ring is composed of a series of possibly related streams occurring throughout the year, reflecting either a true common parental linkage or a common evolutionary end state common to many showers, perhaps driven by the Kozai resonance. Several of these streams also makeup part of the north toroidal sporadic source. That sporadic source, in particular, shows wide variation in strength through the year (Campbell-Brown and Jones, 2006) and we suggest this may reflect the large contributions from these previously unrecognized showers to its activity. More detailed modeling is needed to resolve this linkage. Several of the SDA-complex showers also have a probable link to the previously identified 96P/Machholz complex (cf. Jenniskens, 2006).

The EPG and OCE complexes may also be related to the sporadic ring, though the former is located closer to the inner part of the ring and the latter to the outside of the ring. Notably, many of the showers in the EPG complex are quite weak and all are on Aten-like orbits implying highly evolved orbits (cf. Morbidelli and Gladman, 1998), similar to the LLY complex.

The SMA complex is a series of twin/branch showers which appear to be linked to the Taurid complex, including 2P/Encke, a selection of asteroids and streams (cf. Asher and Clube, 1997). In our data, all streams have radiants in either the helion or anti-helion source with the mean stream orbits showing close linkages to numerous NEAs, many of which are commonly associated with the Taurid complex and 2P/Encke. However, whether all of these are real or chance links is not clear. The NTA and BTA showers also have U and cos Θ values close to this complex, though they fall just barely outside the cluster complex based on our adopted linkage criteria. All these showers seem very probably to have a common

Table 3
Stream members among the seven major complexes identified in our survey.

Complex	IAU/provisional name	Code	$\lambda-\lambda_o$	β	σ_{wave}	a	e	q	i	ω	Ω	U	cos Θ	Parent
EPG	Epsilon Pegasids	EPG	226.5	25.8	41	0.79	0.78	0.17	54	333	105	1.04	−0.65	
	Phi Pegasids	PPEG	313	19.5	10	0.75	0.85	0.11	50	21	54	1.04	−0.68	
	Kappa Cetids	KCET	315.8	−13.6	7	0.75	0.89	0.09	36	198	274	1.00	−0.67	
	Xi Cygnids	XCYG	272.7	43.5	6	0.69	0.47	0.37	68	4	60	1.00	−0.72	
	Psi Pegasids	PSPE	310.5	24.9	5	0.76	0.80	0.15	58	24	63	1.06	−0.68	
LLY	Lambda Lyrids	LLY	248.3	51	42	0.95	0.26	0.70	69	297	41	1.13	−0.59	
	Beta Equuleids	BEQ	221	21.6	36	0.86	0.82	0.15	48	332	107	1.07	−0.61	
	May Vulpeculids	MVUL	238.6	44.6	27	0.88	0.45	0.49	67	312	54	1.10	−0.61	
	Epsilon Aquilids	EAQU	226.5	36.5	21	0.89	0.62	0.34	59	318	54	1.06	−0.59	
	Theta Serpentids	TSER	221	28.7	17	0.93	0.75	0.24	54	323	65	1.08	−0.58	2008 KP
OCE	Southern Daytime omega-Cetids	OCE	331	−13.1	76	1.70	0.92	0.13	35	215	229	1.26	−0.47	
	Northern June Aquilids	NZC	210.6	13.6	45	1.55	0.93	0.12	39	327	101	1.27	−0.50	
	Northern Daytime omega-Cetids	NOC	329.3	12.7	38	1.44	0.92	0.12	35	32	49	1.24	−0.49	
	Alpha Ursae Majorids	AUMA	288.1	54.4	19	1.10	0.21	0.87	71	105	209	1.19	−0.55	
	October kappa Draconids	OKDR	286.7	55.8	17	1.26	0.27	0.92	72	131	216	1.24	−0.54	
	Daytime lambda Taurids	DLT	331.6	−8.4	13	1.50	0.93	0.11	23	212	266	1.21	−0.47	C1733 K1
	Northern delta Aquariids	NDA	208.7	7.8	13	1.70	0.94	0.10	23	330	139	1.27	−0.48	
	Lambda Draconids	LDRA	279.9	56.5	11	1.33	0.26	0.98	73	153	196	1.26	−0.53	
	Xi Draconids	XDR	276.9	57.7	8	1.28	0.23	0.99	72	162	211	1.24	−0.53	
	Microscopiids	MICR	209.8	−12.2	8	1.68	0.94	0.11	37	148	284	1.29	−0.49	
	Tau Ophiuchuiids	TOPH	214.3	17	7	1.24	0.90	0.13	49	328	55	1.24	−0.54	
SMA	South Daytime May Arietids	SMA	343.4	−3.9	34	1.61	0.82	0.30	4	235	234	0.96	−0.28	2001 QJ96
	Southern Taurids	STA	195.6	−4.2	30	1.72	0.82	0.31	5	122	16	0.96	−0.26	2007 RU17
	Daytime zeta Perseids	ZPE	345.5	3.2	22	1.65	0.80	0.33	4	59	74	0.93	−0.25	
	Daytime April Piscids	APS	340.7	3.1	9	1.53	0.84	0.25	5	49	26	1.00	−0.33	2005 NZ6
	Northern iota Aquariids	NIA	197.5	3.4	8	1.57	0.83	0.27	7	308	159	0.98	−0.31	
	Southern iota Aquariids	SIA	197.3	−2.8	5	1.65	0.84	0.27	4	128	320	0.99	−0.30	2005 NZ6
	Daytime kappa Aquariids	MKA	341	2.9	4	1.83	0.87	0.23	5	50	350	1.06	−0.32	2007 KG7
SDA	Southern delta Aquariids	SDA	210.1	−7.6	178	2.20	0.97	0.07	31	154	306	1.39	−0.50	Sungrazers
	Quadrantids	QUA	280.4	63.3	142	3.35	0.71	0.97	72	168	283	1.39	−0.44	2003 EH1
	Daytime Arietids	ARI	329.3	7.5	125	1.75	0.96	0.07	28	26	81	1.34	−0.51	SOHO – 2002 R4
	November omega Orionids	NOO	204.5	−8.1	83	12.01	0.99	0.11	26	142	66	1.44	−0.40	
	December Canis Majorids	DCMA	210.9	−36	50	7.04	0.94	0.44	64	98	86	1.43	−0.41	
	Lambda Bootids	LBO	262.1	54.4	42	1.36	0.29	0.96	78	204	296	1.35	−0.57	
	Alpha Canis Majorids	ACMA	215.8	−40.3	36	3.70	0.86	0.51	67	92	67	1.40	−0.44	
	Xi Coronae Borealids	XCB	302.5	51.2	35	2.84	0.72	0.80	79	124	295	1.49	−0.53	
	Alpha Hydrids	AHY	207.4	−26.4	33	8.62	0.97	0.29	57	116	106	1.43	−0.41	
	Sigma Serpentids	SSE	325.4	20.5	22	1.90	0.92	0.16	62	41	275	1.40	−0.53	
	Daytime kappa Leonids	KLE	335	6.8	21	6.79	0.99	0.09	24	34	183	1.44	−0.43	
	April Sigma Cygnids	ASCY	314.4	55	21	6.51	0.88	0.81	70	126	37	1.41	−0.41	
	November Draconids	NDRA	268.4	62.2	18	3.76	0.74	0.99	75	181	241	1.43	−0.46	2003 EH1
	June Mu Cassiopeids	JMCA	326.7	42.1	17	57.24	0.99	0.58	68	98	74	1.48	−0.41	
	Daytime zeta Cancrids	ZCA	335.1	−4.8	17	4.64	0.98	0.09	17	213	340	1.41	−0.43	
	Piscis Austrinids	PAU	213.5	−18.5	15	3.10	0.96	0.14	66	140	315	1.50	−0.52	
	July Taurids	JTAU	324.6	−20.5	14	1.54	0.90	0.15	61	218	284	1.35	−0.55	
	Daytime xi Orionids	XRI	329.9	−6.2	12	3.24	0.99	0.05	32	203	317	1.48	−0.50	
	Epsilon Perseids	EPE	328.2	16.9	10	4.15	0.97	0.13	62	39	96	1.52	−0.51	96P/Machholz
	Chi Taurids	CTAU	205.8	3.5	8	4.97	0.98	0.08	12	328	220	1.42	−0.43	
	Beta Camelopardalids	BCAM	331.1	38.2	8	67.75	0.99	0.51	64	90	100	1.46	−0.39	
	Beta Pegasids	BPEG	327.4	29.1	7	2.76	0.89	0.30	63	61	36	1.39	−0.47	
	Delta Monocerotids	DEMO	216.3	−33.2	7	3.13	0.88	0.37	70	109	77	1.45	−0.49	
	August Lynxids	ALYN	335	35.7	6	32.65	0.99	0.44	58	82	135	1.41	−0.36	C1402D1
	Rho Bootids	RBOT	317.6	42.9	5	2.64	0.78	0.58	73	93	242	1.42	−0.49	
	Daytime pi Leonids	DPLE	330.9	−4.8	5	2.35	0.98	0.06	20	205	354	1.39	−0.49	
SZC	Southern June Aquilids	SZC	219.8	−13.3	46	1.04	0.94	0.07	56	159	260	1.28	−0.63	
	Theta Coronae Borealids	TCB	282.2	51.5	35	1.04	0.17	0.86	76	98	296	1.25	−0.61	
	Mu Hydrids	MHYD	224.7	−29.3	24	1.08	0.77	0.25	72	136	120	1.29	−0.61	
	Alpha Lacertids	ALA	268.7	50.4	18	1.04	0.03	1.01	81	221	109	1.31	−0.64	
	May Lacertaids	MLAC	319.4	50.2	12	11.14	0.94	0.72	71	115	42	1.46	−0.42	
	January Hydrids	JHYR	228.7	−32.1	12	0.97	0.71	0.28	73	136	112	1.25	−0.64	
	July Andromedids	JAND	310	32.7	10	0.89	0.69	0.27	70	38	101	1.19	−0.64	
	Iota Sculptids	ISC	224.6	−27.6	9	1.02	0.79	0.22	69	142	308	1.26	−0.62	
	Nu Hydrids	NHYD	223.1	−27.3	7	1.04	0.79	0.21	67	140	103	1.24	−0.61	
URS	Ursids	URS	221.1	72.8	35	24.11	0.96	0.95	56	203	270	1.19	−0.19	8P/tuttle
	Gamma Ursae Minorids	GUMI	222.6	75.1	13	4.20	0.77	0.96	51	200	299	1.06	−0.17	8P/tuttle
	Daytime Delta Triangulids	DDTR	351.1	18.5	8	2.95	0.85	0.45	20	78	53	0.97	−0.14	2002 SQ41 (Secular)
	Beta Monocerotids	BMON	191.3	−31.8	8	3.84	0.86	0.53	33	90	91	1.04	−0.16	2005 UJ159

progenitor and interestingly do not overlap in their periods of activity, yet are active for a total of almost half a year. From simulations, Wiegert et al. (2009) and Stohl (1986) have suggested that most of the sporadic activity from the helion/anti-helion sources originates from 2P/Encke; possibly the SMA complex represents linked coherent streams in the broader Taurid complex.

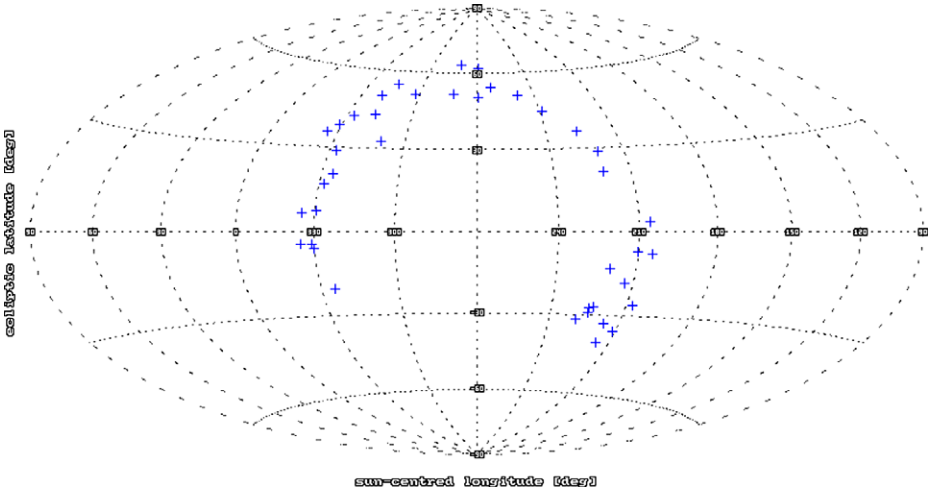

Fig. 7. Radiant locations at the time of maxima in sun-centered ecliptic coordinates for showers linked to the LLY, SZC and SDA complexes. These shower radiants follow the sporadic "ring" first identified by Campbell-Brown (2008).

Finally, a cluster of four showers linked to the Ursids is particularly noteworthy. First, the newly identified Gamma Ursae Minorids (GUM) has a radiant only a few degrees from the Ursid radiant in sun-centered ecliptic coordinates, a similar speed and occurs less than 20 days after the peak of the Ursid shower. We note that the Ursid velocity is systematically underestimated in our data because of poor radiant geometry relative to our remote link directions, a systematic bias first noted in paper I. It is not clear how this shower may relate to the Ursids and 8P/Tuttle – it might be a random interloper or may hint at a more complex evolutionary link between the showers and 8P/Tuttle. Also linked to these showers via possible secular evolutionary tracks is the Beta Monocerotids, a shower occurring at the same time as the peak of the Ursids and somewhat unusual in that a search for possible parents produced a strong link ($D' < 0.05$) with the Asteroid 2005 UJ159 at close to the 95% confidence level (Wiegert and Brown, 2004). Similarly, the fourth shower in this complex, the Daytime Delta Triangulids, has a plausible link to 2002 SQ41 based on comparison of secular invariants of the two orbits. This complex hints at an old, large scale disintegration possibly associated with the evolution of 8P/Tuttle, but more detailed simulations are clearly needed.

5.2. Individual stream linkages: parent bodies and other showers

The second approach we use to generate possible interstream linkages and links to parent bodies is the standard orbital clustering discriminant, the D-criterion (Drummond, 1981). Table 4 shows streams and their potential parent bodies linked in this manner. We adopt a $D' < 0.1$ as significant, noting that errors in radiant location and speed make this a somewhat arbitrary choice. Many of these shower associations may be one single stream that our linking algorithm has identified as two separate streams (e.g. PSP and PHP) but where the activity level drops below our 3σ threshold for some days between the showers or where low activity levels lead to radiant uncertainties of more than 3° effectively cutting the shower linkage chain. We term these associated showers in the table. Showers showing similar orbits, but having widely separated periods of activity (not obvious twins or branches) we term linked, while individual streams with multiple Earth intersections as described earlier are listed as branches or twins with other streams in the table.

Some significant, new possible linkages not yet discussed in other literature or found in paper I include:

1. *Theta Serpentids (TSR) and 2008 KP*: the newly recognized TSR shower is both strong and fairly long-lived – it is unquestionably a real shower and shows noticeable enhancement relative to the background for almost 3 weeks. It shows a possible link ($D' < 0.1$) to Asteroid 2008 KP (absolute magnitude of +18.8 corresponding to a diameter between 0.5 and 1.1 km, MPEC 2008-K45), which is on a similar high-inclination orbit. Interestingly, while asteroid – stream associations are not uncommon at this significance level, such a close link at high inclinations is very unusual. Using the criteria outlined in Wiegert and Brown (2004) we find the orbital similarity at this level is unlikely to be random chance at close to the 90% certainty level. Such a finding suggests 2008 KP to be a prime candidate as a recently extinct cometary nucleus and warrants follow-on physical observations.
2. *August Lyncids (ALN) and Comet C1402 D1*: the new ALN minor shower is detectable over a 3 week period, though it is only of modest activity relative to the background for most of this time. However, the 6σ detection at the time of maximum is clearly significant and examination of the yearly background level of activity at this ecliptic radiant location shows the peak very clearly. The association with the great daylight comet of 1402 is at a level better than $D' < 0.09$ and is one of the best comet – shower linkages in our survey. The nodal longitudes of the shower and comet, in particular, agree to better than 0.5°. This comet is notable as having been visible in daylight longer than any comet in history. However, the precision of the orbit is not good (Kronk, 1999) so the significance of this association, while interesting, is questionable.
3. *Quadrantids (QUA) and November I Draconids (NID)*: a surprising finding from our survey is an apparently new shower (NID) that appears to be directly associated with the Quadrantids. The NID has the same radiant location (in ecliptic coordinates) and speed as the QUA and both have overlapping periods of activity. Indeed, our automatic algorithm linked portions of the showers as though they were a single long-duration shower, extending the QUA period of activity into November. From our observations, we interpret the NID as simply an early extension of the QUA. Fig. 8 shows the combined NID/QUA radiant drift, activity and velocity variation with the match in radiant drift and velocity being good. Near the QUA maximum some deviation in the apparent rate of change of the dec drift and drift in V_g is apparent. We speculate this may reflect two different components in the stream – a long-lived, low-level of activity prior to QUA

Table 4
Possible interstream linkages and stream-parent body links based on orbital similarity using the D'-criterion (Drummond, 1981).

IAU code	λ_{max}	a	e	q	i	ω	Ω	Shower linkages (twins/branches)	Possible parent bodies
BTA	94	1.94	0.80	0.38	4	246	274	Linked with the NTA?	2007 UL12 (Taurid complex)
NTA	219	2.06	0.83	0.35	0	115	39	North branch to STA	2007 RU17
PHP	54	0.75	0.85	0.11	50	21	54	Associated with PSP	
PSP	63	0.76	0.80	0.15	58	24	63	Associated with PHP	
EPG	105	0.79	0.78	0.17	54	333	105	Associated with BEQ	
TSR	65	0.93	0.75	0.24	54	323	65		2008 KP
BEQ	107	0.86	0.82	0.156	48	332	107	Associated with EPG	
NOC	49	1.44	0.92	0.12	35	32	49	North branch to OCE	
OCE	49	1.70	0.92	0.13	35	215	229	South branch to NOC	
DLT	86	1.50	0.93	0.11	23	212	266	Twin of GEM?	C1733 K1
NZC	101	1.55	0.93	0.12	40	327	101	North branch to MIC	
MIC	104	1.68	0.94	0.11	37	148	284	South branch to NZC	Linked to start of SDA?
XDR	211	1.28	0.23	0.99	72	162	211	Associated with OKD	
OKD	216	1.26	0.27	0.92	72	131	216	Link with LDR	
APS	26	1.53	0.84	0.25	5	49	26	Link with NIA/SIA?	2005 NZ6
SMA	54	1.61	0.82	0.30	4	235	234	South branch to ZPE; linked to NIA/SIA	2001 QJ96
ZPE	74	1.65	0.80	0.33	4	59	74	North branch to SMA; linked to STA/NTA	
SIA	140	1.65	0.84	0.27	4	128	320	South branch to NIA	2005 NZ6
NIA	159	1.57	0.83	0.27	7	308	159	North branch to SIA; linked to SMA	
STA	196	1.72	0.82	0.31	5	122	16	South branch to NTA; link with SMA/ZPE	2007 RU17
MKA	350	1.83	0.87	0.23	5	50	350		2007 KG7
ARC	37	6.51	0.88	0.81	70	126	37	Associated with MAL	
JMC	74	57.24	0.99	0.58	68	98	74	Twin of RBO?	
ARI	81	1.75	0.96	0.07	28	26	81		Sungrazers (SOHO – 2002R4)
EPE	96	4.15	0.97	0.13	62	39	96		96P/Machholz
ALN	135	32.65	0.99	0.44	58	82	135		C1402 D1
ZCA	160	4.64	0.98	0.09	17	213	340	Twin of CTA	
CTA	220	4.97	0.98	0.08	12	329	220	Twin of ZCA	
NID	241	3.76	0.74	0.99	75	181	241	Associated with QUA	2003 EH1 or 12P/Pons-Brooks
RBO	242	2.64	0.78	0.58	73	93	242	Twin of JMC?	
GCM	257	3.13	0.88	0.37	70	109	77	Associated with DCM	
DCM	266	7.04	0.94	0.44	64	98	86	Associated with GCM	
QUA	283	3.35	0.71	0.97	72	168	283	Associated with NID	2003 EH1
LBO	296	1.36	0.29	0.96	78	204	296	Linked to ALA?	
MAL	42	11.14	0.94	0.72	71	115	42	Associated with ARC	
ALA	109	1.04	0.03	1.01	81	221	109	Linked with LBO?	
ISC	128	1.02	0.79	0.22	69	142	308	Linked with KHY/JHY	
KHY	283	1.04	0.79	0.21	67	140	103	Associated with JHY/MHY; linked with ISC	
JHY	292	0.97	0.71	0.28	73	136	112	Associated with MHY/KHY; linked with ISC	
MHY	300	1.08	0.77	0.25	72	136	120	Associated with JHY/KHY; link with ISC	
DDT	53	2.95	0.85	0.45	20	78	53		2002 SQ41
URS	270	24.11	0.96	0.95	56	203	270	Associated with GUM?	8P/Tuttle
BMO	271	3.84	0.86	0.53	33	90	91		2005 UJ159
GUM	299	4.20	0.77	0.96	51	200	299	Associated with URS?	8P/Tuttle
LYR	32	10.85	0.92	0.91	80	216	32		C/1861 G1 (Thatcher)
ETA	45	4.14	0.87	0.52	163	88	45	Twin of ORI	1P/Halley
DTR	46	4.24	0.87	0.56	16	93	46	Twin of OER	
XIC	54	1.00	0.55	0.45	4	236	234		2008 OX2
TPR	106	4.53	0.90	0.46	104	81	106	Twin of DHY?	
CAP	123	2.26	0.74	0.58	7	270	123	Twin of DCS	169P/NEAT (2002 EX12)
PER	140	−9.91	1.10	0.96	116	153.	140		109P/Swift–Tuttle
DSX	186	1.07	0.86	0.15	22	213	6	Link with GEM	155140 (2005 UD)
ORI	208	5.47	0.90	0.57	163	84	28	Twin of ETA	1P/Halley
LMI	210	4.63	0.88	0.58	125	96	210		C1739 K1
OER	227	2.63	0.80	0.52	18	94	47	Twin of DTR	1999 VK12
LEO	237	2.52	0.61	0.98	162	171	237		55P/Tempel–Tuttle
THA	237	1.13	0.90	0.12	28	330	237	Associated with GEM	2004 QX2
GEM	261	1.35	0.90	0.14	23	325	261	Twin of DLT?; link with DSX?; associated with THA	3200 Phathon
MON	261	8.88	0.98	0.19	32	129	81		D/1917 F1 (Mellish)
DHY	266	4.82	0.92	0.41	106	103	86	Twin of TPR?	
JLE	282	5.34	0.99	0.05	108	335	282		SOHO (2005D1)
XSA	288	2.18	0.78	0.47	6	79	288		2002 AU5
CVN	293	9.40	0.91	0.87	93	222	293		C/1975 XI or C/1999 A1
DCS	301	2.67	0.79	0.56	7	271	121	Twin of CAP	169P/NEAT (2002 EX12)

maximum probably related to older ejections and the younger QUA "core" producing the sharp, well-known peak in early January. If truly there is an extension of QUA activity over a full 2 months, it would strongly support the notion that the QUA and 2003 EH1, the probable parent (Jenniskens, 2006), are part of a broader and older stream complex perhaps with 2003 EH1 and 96P/Machholz as members (Babadzhanov and Obrubov, 1992; Jones and Jones, 1993). We note that the NID shower identified is similar to the recently described December Alpha Draconids (IAU 334) (SonotaCo, 2009), though our time of maximum and radiant drift differ significantly.

4. *The Daytime Triangulids (DTR) and Omicron Eridanids (OER)*: these two new showers identified in our survey are both near the limit of our detection criteria, with the DTR lasting only 3 days significantly above background. However, these showers are clearly twin streams which provides an independent check

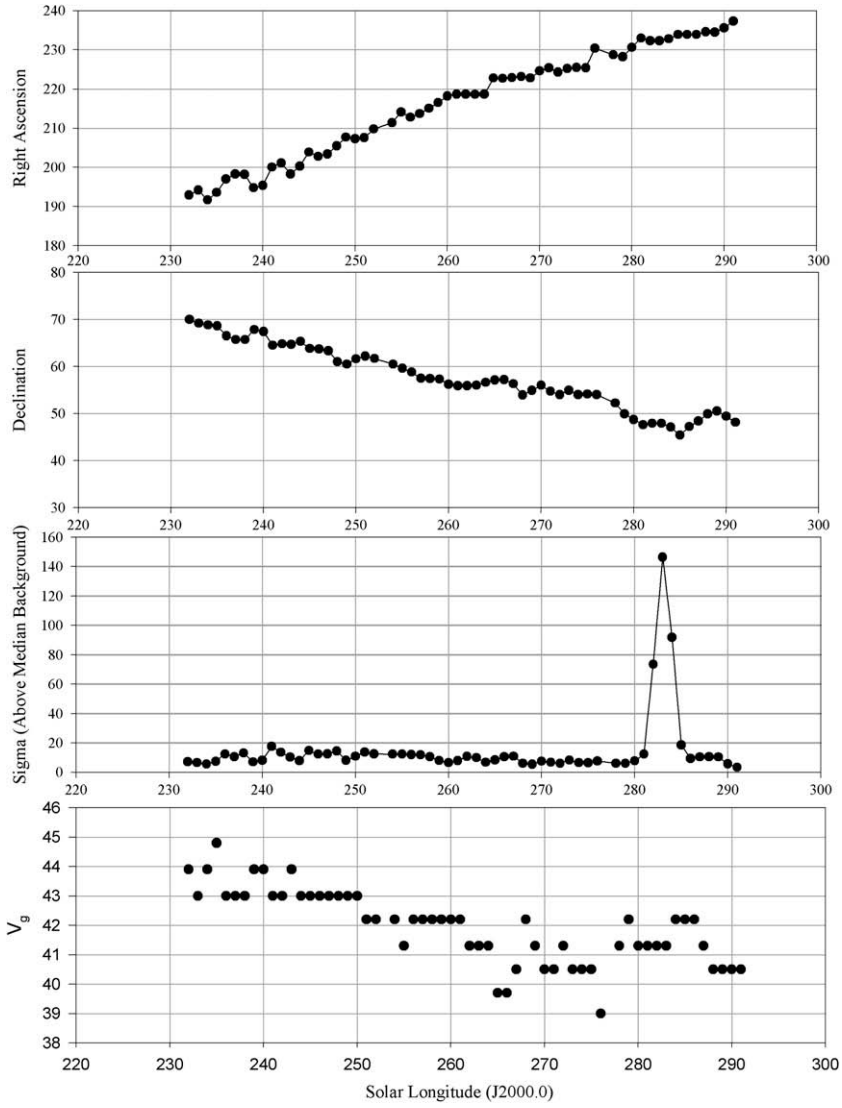

Fig. 8. The radiant drift (top two plots), activity levels (second from bottom) and estimated velocity (bottom plot) for the QUA–NID stream. Note that the "traditional", sharp annual QUA shower lasts from $\lambda = 281°$ to 285° and is likely the youngest part of the broader QUA complex.

on the reality of our shower selections at these very low activity levels. The apparent link to 1999 VK12 ($D' = 0.08$) should not be taken as particularly significant as our model (Wiegert and Brown, 2004) suggests a 25% likelihood of chance association at this level with random background NEAs.

5. *Alpha Capricornids (CAP) and Daytime Chi Capricornids (DCS)*: Jenniskens (2006) noted that CAP shower having $\omega = 270°$ should have an ascending nodal intersection with the Earth and therefore a detectable Daytime twin stream. Based on older radar data establishing the orbital elements of the DCS shower, he rejected this as a probable twin, though the timing of the shower was approximately correct for the southern CAP twin. Re-examination of our continuous radar survey records, shows a stream peaking about 10 days earlier than is listed for the DCS but with similar velocity, most similar to stream 2.01 in Gartrell and Elford (1975) and the Chi Capricornids given by Sekanina (1973), though the velocity is 3–4 km/s lower. With our significantly revised radiant location and speed relative to the original DCS value from Jenniskens (2006), the orbit is a clear match for the southern twin for the CAP. The characteristics of this new DCS shower, together with those of the CAP provide a strong observational constraint to models for formation and evolution of these streams and linkages to parent bodies.
6. *November Theta Aurigids (NTA) and Geminids (GEM)*: our survey algorithm identified an apparently new shower of 1 week duration beginning in mid-November. The shower has very similar characteristics to the Geminids which peaks a month later. Moreover, extension of the radiant drift from the time of the NTA shower maximum produces a predicted radiant (within 95% confidence limits) directly on the GEM radiant. Examining the raw data, it seems likely that this represents an early extension of the GEM shower in our data – the drop off between the end of the NTA and the GEM reflecting again a decrease below our chosen cutoff. Fig. 9 shows the absolute values of the wavelet coefficient at the ecliptic radiant coordinates of the GEM. Our criteria (3σ above background) clearly truncates the full period of detectable activity in our data. To the background activity level, we find the GEM period of activity to extend from $\lambda = 225°$ to 282°; or roughly from November 7 to January 2 each year, much longer than the accepted duration of the shower (taken to be from late November/early December to mid-December typically; cf. Jenniskens, 2006; Rendtel and Arlt, 2008). Sekanina (1970), in the only other major radar orbital survey to record large numbers of Geminids, reported a duration from November 30 to December 29. It seems the stream is much broader and longer-lived at smaller radar particle sizes than has previously been appreciated.

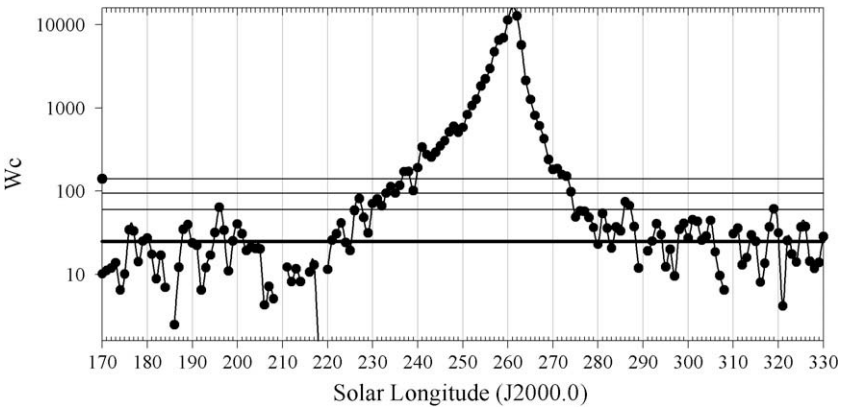

Fig. 9. The wavelet coefficient values centered at the location of the Geminid shower maximum (in sun-centered ecliptic coordinates) throughout the year. The horizontal bold line represents the median wavelet values over the year while each successive horizontal line above this level is an additional one standard deviation in the yearly mean activity levels. Note that the ordinate is logarithmic.

7. *The Canum Venaticids and C/1975 X1 (Sato)*: the newly recognized Canum Venaticids show clear activity from January 10 to January 17 using our shower identification algorithm. Examination of the raw wavelet data shows the stream to be visible well above the background until the end of January. The shower has a potential link to C/1975 X1 with the D' linkage value being possibly as good as 0.08 given the measurement uncertainty of the shower orbit, making it among the best shower-long period comet links in our survey.

6. Conclusions

Using three million individual orbits measured during 7 years of operation of the CMOR radar we have identified 117 meteor showers active for at least 3 days each year through application of a 3D wavelet search algorithm. These streams include 42 of the 45 previously identified major streams from our first survey summarized in paper I. Removing a number of possible duplicate showers we have a lower limit of 109 total streams (42 identified in paper I and at least 62 newly identified streams). We find evidence among these streams for seven "complexes" of showers possibly linked to common progenitor(s) through secular invariants. Among these complexes are seven showers in the SMA complex linked to the Taurids and suggestive that Taurid-related activity occurs over a substantial fraction of the entire year, a point also noted in paper I, lending support to the notion that the Taurid complex as a primary contributor of meteor activity throughout the year. The LLY, SDA, and SZC complexes have radiants lining the sporadic "ring" feature identified in earlier works examining sporadic radiant distributions from CMOR, suggestive of an underlying coherent stream component to this feature which may also provide some constraints for possible physical models of the ring. We have also detected a series of three new showers apparently related to the Ursid stream and possibly 8P/Tuttle; the origin and evolution of the Ursids and 8P/Tuttle should be re-examined in light of these new showers. We caution that the reality of these complexes and specific stream memberships still needs to be more firmly established through dynamical simulations.

We also find much longer than previously reported periods of activity for the Quadrantids (early November–mid-January) and the Geminids (early November–January) at our small radar particle sizes. We emphasize that the 3D wavelet approach used in our study allows detections down to very low activity levels, perhaps explaining why such long activity periods for these showers have not been previously reported.

The newly recognized Theta Serpentid shower has the most significant orbital link to an NEA (2008 KP) of any new stream in our survey, suggesting strongly that it may be a relatively recently dormant cometary nucleus.

Finally, among the many new twins and stream branches identified in our shower database is the southern twin for the Alpha Capricornid stream: the characteristics of these two streams together should provide strong constraints for formation models of the common Alpha Capricornid stream.

The next stage in our long-term radar shower survey program will include multi-year fluxes and mass distribution indices for some of the major radar showers. We also intend to examine the handful of unusually strong outbursts lasting for less than 1 day that have occurred over the last 7 years but have not yet studied in detail. The CMOR radar is being upgraded to include three additional outlying stations in the summer of 2009 and it is our expectation that this new CMOR II system will provide higher precision orbits and possibly deceleration data for a large sample of the showers identified in our first two survey papers. It is hoped that this survey program, which has resulted in the identification of a suite of showers from a common dataset using consistent search criteria and ultimately supplemented with physical information (such as bulk densities), will provide the motivation and partial observational basis for theoretical studies of the origin and evolution of some of the many unusual meteor showers documented in this program.

Acknowledgments

PGB thanks the Canada Research Chair Program, the Natural Sciences and Engineering Research Council and the NASA Meteoroid Environment Office for funding support. The authors gratefully acknowledge the invaluable technical assistance of K. Ellis and Z. Krzeminski in day to day radar operations and ongoing helpful guidance of J. Jones and A.R. Webster. D.J. Asher and V. Porubcan provided very helpful reviews of an earlier version of this work.

References

Asher, D.J., 1999. The Leonid meteor storms of 1833 and 1966. Mon. Not. R. Astron. Soc. 307, 919–924.
Asher, D.J., Clube, S.V.M., 1997. Towards a dynamical history of 'Proto-Encke'. Celest. Mech. Dynam. Astron. 69, 149–170.
Asher, D.J., Izumi, K., 1998. Meteor observation in Japan: New implications for a Taurid meteoroid swarm. Mon. Not. R. Astron. Soc. 297, 23–27.
Babadzhanov, P.B., Obrubov, Y., 1992. Evolution of short-period meteoroid streams. Celest. Mech. Dynam. Astron. 54, 111–127.

Babadzhanov, P.B., Williams, I.P., Kokhirova, G.I., 2008. Near-Earth Objects in the Taurid complex. Mon. Not. R. Astron. Soc. 386, 2271–2277.
Beech, M., 1990. William Frederick Denning: In quest of meteors. J. R. Astron. Soc. Canada 84, 383–396.
Brown, P., Jones, J., 1998. Simulation of the formation and evolution of the Perseid meteoroid stream. Icarus 133, 36–68.
Brown, P., Jones, J., Weryk, R.J., Campbell-Brown, M.D., 2004. The velocity distribution of meteoroids at the Earth as measured by the Canadian Meteor Orbit Radar (CMOR). Earth Moon Planets 95, 617–626.
Brown, P., Weryk, R.J., Wong, D.K., Jones, J., 2008. A meteoroid stream survey using the Canadian Meteor Orbit Radar. I. Methodology and radiant catalogue. Icarus 195, 317–339.
Campbell-Brown, M.D., 2008. High resolution radiant distribution and orbits of sporadic radar meteoroids. Icarus 196, 144–163.
Campbell-Brown, M., Jones, J., 2006. Annual variation of sporadic radar meteor rates. Mon. Not. R. Astron. Soc. 367, 709–716.
Ceplecha, Z., 1987. Geometric, dynamic, orbital and photometric data on meteoroids from photographic fireball networks. Bull. Astron. Inst. Czechos. 38, 222–234.
Ceplecha, Z., Borovička, J., Elford, W.G., ReVelle, D.O., Hawkes, R.L., Porubčan, V., Šimek, M., 1998. Meteor phenomena and bodies. Space Sci. Rev. 84, 327–471.
Chambers, J.E., 1999. A hybrid symplectic integrator that permits close encounters between massive bodies. Mon. Not. R. Astron. Soc. 304, 793–799.
Drummond, J.D., 1981. A test of comet and meteor shower associations. Icarus 45, 545–553.
Gartrell, G., Elford, W.G., 1975. Southern hemisphere meteor stream determinations. Aust. J. Phys. 28, 591–620.
Morbidelli, A., Gladman, B., 1998. Orbital and temporal distributions of meteorites originating in the asteroid belt. Meteor. Planet. Sci. 33, 999–1016.
Graps, A., 1995. An introduction to wavelets. IEEE Comput. Sci. Eng. 2, 50–68.
Green, D.W.E. 2008. Catalogue of Cometary Orbits 2008, International Astronomical Union Circular 8958.
Hocking, W.K., Fuller, B., Vandepeer, B., 2001. Real-time determination of meteor-related parameters utilizing modern digital technology. J. Atmos. Terr. Phys. 63, 155–169.
Jenniskens, P., 2006. Meteor Showers and their Parent Comets. Cambridge University Press. 790 pp.
Jenniskens, P., Jopek, T.J., Rendtel, J., Porubcan, V., Spurny, P., Baggaley, J., Abe, S., Hawkes, R., 2009. On how to report new meteor showers. WGN J. Int. Meteor Organ. 37, 19–20.
Jones, J., 1985. The structure of the Geminid meteor stream. I – The effect of planetary perturbations. Mon. Not. R. Astron. Soc. 217, 523–532.
Jones, W., 1997. Theoretical and observational determinations of the ionization coefficient of meteors. Mon. Not. R. Astron. Soc. 288, 995–1003.
Jones, J., Brown, P., 1993. Sporadic meteor radiant distributions – Orbital survey results. Mon. Not. R. Astron. Soc. 265, 524–532.
Jones, J., Jones, W., 1993. Comet Machholz and the Quadrantid meteor stream. Mon. Not. R. Astron. Soc. 261, 605–611.
Jones, J., Brown, P., Ellis, K.J., Webster, A.R., Campbell-Brown, M.D., Krzemenski, Z., Weryk, R.J., 2005. The Canadian Meteor Orbit Radar (CMOR): System overview and preliminary results. Planet. Space Sci. 53, 413–421.
Jopek, T.J., Valsecchi, G.B., Froeschle, C., 1999. Meteoroid stream identification: A new approach – II. Application to 865 photographic meteor orbits. Mon. Not. R. Astron. Soc. 304, 751–758.
Kresak, L., Porubcan, V., 1970. The dispersion of meteors in meteor streams. I. The size of the radiant areas. Bull. Astron. Inst. Czechos. 21, 153–170.
Kronk, G.W., 1999. Cometography: A Catalog of Comets. Ancient – 1799, vol. 1. Cambridge University Press, Cambridge. 563 pp.
Levison, H., 1996. Comet taxonomy. In: Rettig, T.W., Hahn, J.M. (Eds.), Completing the Inventory of the Solar System, Astronomical Society of the Pacific Conference Proceedings, vol. 107, pp. 173–191.
Molau, S., 2007. How good is the IMO working list of meteor showers? A complete analysis of the IMO video meteor database. In: Proc. Int. Meteor Conf. 2006, International Meteor Organization.
Rendtel, J., Arlt, R. (Eds.), 2008. Handbook for Meteor Observers. International Meteor Organization, Potsdam. 190 pp.
Sekanina, Z., 1970. Statistical model of meteor streams. II. Major showers. Icarus 13, 475–493.
Sekanina, Z., 1973. Statistical model of meteor streams. III. Stream search among 19303 radio meteors. Icarus 18, 253–284.
SonotaCo, 2009. A meteor shower catalog based on video observations in 2007–2008. WGN: J. Int. Meteor Organ. 37, 55–62.
Stohl, J., 1986. The distribution of sporadic meteor radiants and orbits. In: Lagerkvist, C.I., Rickman, H., Lindblad, B.A., Lundstedt, H. (Eds.), Asteroids, Comets and Meteors II, Proceedings of the International Meeting, Uppsala, Sweden, June 3–6, 1985, pp. 565–574.
Valsecchi, G.B., Jopek, T.J., Froeschle, C., 1999. Meteoroid stream identification: A new approach – I. Theory. Mon. Not. R. Astron. Soc. 304, 743–750.
Verniani, F., 1973. An analysis of the physical parameters of 5759 faint radio meteors. J. Geophys. Res. 78, 8429–8462.
Webster, A.R., Brown, P.G., Jones, J., Ellis, K.J., Campbell-Brown, M., 2004. Canadian Meteor Orbit Radar (CMOR). Atmos. Chem. Phys. Discuss. 4, 1181–1201.
Whipple, F.L., 1940. Photographic meteor studies. III. The Taurid meteor shower. Proc. Am. Phil. Soc. 83, 711–745.
Wiegert, P., Brown, P., 2004. The problem of linking minor meteor showers to their parent bodies: Initial considerations. Earth Moon Planets 95, 19–26.
Wiegert, P., Vaubaillon, J., Campbell-Brown, M.D., 2009. A dynamical model of the sporadic meteoroid complex. Icarus 201, 295–310.
Wisdom, J., Holman, M., 1991. Symplectic maps for the *n*-body problem. Astron. J. 102, 1528–1538.